VIROLOGY

# Norovirus co-opts NINJ1 for selective protein secretion

**Jaewon Song[1], Li Zhang[1], Seokoh Moon[1], Ariana Fang[1], Guoxun Wang[2,3], Newsha Gheshm[1], Skylar A. Loeb[1], Paul Cao[4], Joselynn R. Wallace[4], Mia Madel Alfajaro[5], Madison S. Strine[6], Wandy L. Beatty[7], Amanda M. Jamieson[1], Robert C. Orchard[2,3], Bridget A. Robinson[8], Timothy J. Nice[8], Craig B. Wilen[5,6], Anthony Orvedahl[9,10], Tiffany A. Reese[2,3], Sanghyun Lee[1]***



**Plasma membrane rupture by Ninjurin-1 (NINJ1) executes programmed cell death, releasing large cellular damage-associated molecular patterns (DAMPs). However, the regulation and selectivity of NINJ1-mediated DAMP release remain unexplored. Here, we uncover that murine norovirus (MNoV) strategically co-opts NINJ1 to selectively release the intracellular viral protein NS1, while NINJ1-mediated plasma membrane rupture simultaneously bulk-releases various cellular DAMPs. Host caspase-3 cleaves the precursor NS1/2, leading to NS1 secretion via an unconventional pathway. An unbiased CRISPR screen identifies NINJ1 as an essential factor for NS1 secretion. During infection, NINJ1 is recruited to the viral replication site, where it oligomerizes and forms speckled bodies, directly interacting with NS1. Subsequent mutagenesis studies identify critical amino acid residues of NS1 necessary for its interaction with NINJ1 and selective secretion. Genetic ablation or pharmaceutical inhibition of caspase-3 inhibits oral MNoV infection in mice. This study underscores the co-option of NINJ1 for controlled release of an intracellular viral protein.**

## INTRODUCTION

Plasma membrane rupture was long thought to be driven by osmotic pressure, but the discovery of Ninjurin-1 (NINJ1) has revealed it as a regulated process during the execution phase of programmed cell death pathways such as apoptosis and pyroptosis (*1*). Self-oligomerization of NINJ1 at the plasma membrane triggers membrane rupture, leading to the release of intracellular damage-associated molecular patterns (DAMPs) (*2*–*4*). While gasdermin pores are recognized as channels for small proteins (<20 kD), NINJ1-mediated plasma membrane rupture is proposed as a mechanism for nonspecific bulk release of larger DAMP proteins [e.g., lactate dehydrogenase (LDH), 140 kD]. However, the control of cellular DAMP release by NINJ1 and its potential selectivity remain largely unexplored.

Murine norovirus (MNoV), a nonenveloped enteric virus, encodes the small nonstructural protein NS1 (15 kD), which suppresses interferon-λ (IFN-λ) responses in trans in the intestine (*5*). Type III IFN-λ has been identified as a critical host immune determinant controlling norovirus infection in the intestine (*6*, *7*). Noroviruses have also evolved to tolerate or evade IFN-λ. MNoV does so by secreting the viral protein NS1 (*5*). Despite lacking a signal sequence, NS1 is secreted upon the caspase-3 cleavage of the precursor protein NS1/2 using an unconventional secretion pathway yet to be identified (*5*). The precursor NS1/2 is localized to the endoplasmic reticulum (ER) and the membranous viral replication complex (*8*, *9*). It has been shown that NS1 is secreted as a soluble protein, not incorporated into virions or vesicles using size exclusion chromatography (*5*). Recent findings reveal that NS3 protein in MNoV, a viral mimic of cellular mixed lineage kinase domain-like (MLKL), drives apoptosis through mitochondrial permeabilization, elucidating the upstream mechanistic details of cellular death induction by MNoV infection (*10*). In this study, we report that viral regulation of apoptosis and NINJ1 serves as a specific secretion pathway for NS1. We also highlight the physiological relevance of this regulation in vivo.

## RESULTS

### Mucosal epithelial infection of MNoV in tuft cells requires host caspase-3

Different MNoV strains have distinct cell and tissue tropisms, which we leverage to elucidate the role of secreted NS1 and the requirement of cellular death factors. There are two distinct cell tropisms of MNoV in the intestine: (i) mucosal intestinal epithelial infection in tuft cells and (ii) submucosal and systemic infection in hematopoietic cells (*11*–*16*). Two model strains of MNoV were used in this study: a persistent strain, CR6, and an acute strain, CW3. These two model strains display nonoverlapping cell tropism in enteric pathogenesis (*13*, *14*, *17*–*19*). Peroral infection with CR6 exclusively results in mucosal epithelial infection in tuft cells in the intestine (*13*). CR6 replication in the intestine persists for several weeks. While CR6 evades clearance by T cell and B-cell responses, it is primarily controlled by IFN-λ immunity (*5*–*7*, *19*–*23*). Evasion of IFN-λ immunity by secreted NS1 is essential for establishing infection in tuft cells, enabling persistence (*5*). In contrast, the acute strain CW3 models acute submucosal intestinal, and systemic norovirus infection. Peroral infection with CW3 results in multiple infected cell types including myeloid cells (i.e., macrophages and dendritic cells) and B cells (*14*, *16*, *24*–*26*). Intraperitoneal delivery of CR6 into mice enables hematopoietic cell infection with minimal tuft cell infection in the intestine (see the model in fig. S1A). While CW3 and CR6 have distinct cell tropisms in vivo, both viruses readily infect tuft cells and myeloid cells in vitro. By using an enteroid culture system

[1]Department of Molecular Microbiology and Immunology, Division of Biology and Medicine, Brown University, Providence, RI 02912, USA. [2]Department of Immunology, University of Texas Southwestern Medical Center, Dallas, TX 75390, USA. [3]Department of Microbiology, University of Texas Southwestern Medical Center, Dallas, TX 75390, USA. [4]Center for Computational Biology of Human Disease and Center for Computation and Visualization, Brown University, Providence, RI 02912, USA. [5]Department of Laboratory Medicine, Yale University, New Haven, CT 06520, USA. [6]Department of Immunobiology, Yale University, New Haven, CT 06520, USA. [7]Department of Molecular Microbiology, Washington University School of Medicine in St. Louis, St. Louis, MO 63110, USA. [8]Department of Molecular Microbiology and Immunology, Oregon Health & Science University, Portland, OR 97239, USA. [9]Department of Pediatrics, Washington University School of Medicine in St. Louis, St. Louis, MO 63110, USA. [10]Department of Pathology and Immunology, Washington University School of Medicine in St. Louis, St. Louis, MO 63110, USA.
*Corresponding author. Email: sanghyun_lee@brown.edu

harboring differentiated tuft cells (*27*), we confirmed that both CR6 and CW3 strains secrete NS1 from the infected cells (fig. S1B).

To determine the physiological role of cellular factors for programmed cell death during MNoV infection, we used genetic knockout (KO) mouse models. Strikingly, in *Casp3*$^{-/-}$ mice, no detectible viruses were observed in the intestine and the mesenteric lymph nodes (MLNs) or the feces after the peroral CR6 challenge (Fig. 1, A and B). The defect in viral infection in *Casp3*$^{-/-}$ animals is specific to intestinal epithelial infection in tuft cells since peroral CW3 and intraperitoneal CR6 had no or minimal defects in viral replication in intestinal and systemic organs in these animals (Fig. 1, D and F). As expected, these two myeloid tropic infection models showed minimal viral shedding into the feces (Fig. 1, C and E).

We confirmed that the deficiency of some inflammasome components (i.e., *Casp1*$^{-/-}$*Casp4*$^{-/-}$) or gasdermin D and/or gasdermin E (i.e., *Gsdmd*$^{-/-}$, *Gsdme*$^{-/-}$, and *Gsdmd*$^{-/-}$*Gsdme*$^{-/-}$) did not affect peroral CR6, peroral CW3, or intraperitoneal CR6, with the exception of marginally increased viral replication in *Gsdmd*$^{-/-}$ tissue, reduced viral shedding from *Gsdmd*$^{-/-}$*Gsdme*$^{-/-}$ mice during intestinal infection, and increased viral replication in *Gsdmd*$^{-/-}$*Gsdme*$^{-/-}$ spleen and fecal shedding in *Gsdme*$^{-/-}$ with a systemic infection model (fig. S1, C to M). In *Stat1*$^{-/-}$ mice, NLRP3 inflammasome–driven interleukin-1β (IL-1β) contributes to acute lethal infection of peroral CW3 (*28*, *29*), which is likely due to the uncontrolled viremia in the immunodeficient host. In immunocompetent animal hosts shown in this study, the contribution or requirement of inflammasome and gasdermins for both acute and persistent MNoV infection was minimal. Collectively, these data indicate the specific requirement of caspase-3 for MNoV infection in intestinal tuft cells. These results align with the previous findings that the caspase-3 cleavage–defective CR6 virus (CR6$^{D121/131G}$) loses the peroral infectivity but retains the intraperitoneal infectivity in wild-type (WT) mice (*5*, *30*). We confirmed that CR6$^{D121/131G}$ virus, produced independently by two separate groups, exhibited rescued intestinal replication in IFN-λ receptor–deficient (*Ifnlr1*$^{-/-}$) mice, which is in agreement with the previous report and supports the crucial role of secreted NS1 in resisting host IFN-λ responses (fig. S1N) (*5*). In summary, caspase-3 activity and NS1 release are critical for mucosal intestinal MNoV infection in tuft cells.

## NS1 is effectively secreted from MNoV-replicating cells, resulting in "NS1-absent" cells

Using a flow cytometry assay with antibodies against intracellular nonstructural proteins NS1 and NS6/7, we observed an interesting phenomenon (Fig. 2A). During viral infection in BV2 cells, an MNoV-permissive microglial cell line, we observed a distinct NS1-negative population among MNoV-infected cells (Fig. 2B). The MNoV-infected cells are NS1$^{+}$NS6/7$^{+}$ double positive (NS1$^{+}$ hereafter) at the early and mid-phase of viral replication (modeled in Fig. 2A). At the late phase of viral replication (12 ~ 18 hours post-infection, hpi), NS1$^{-}$NS6/7$^{+}$

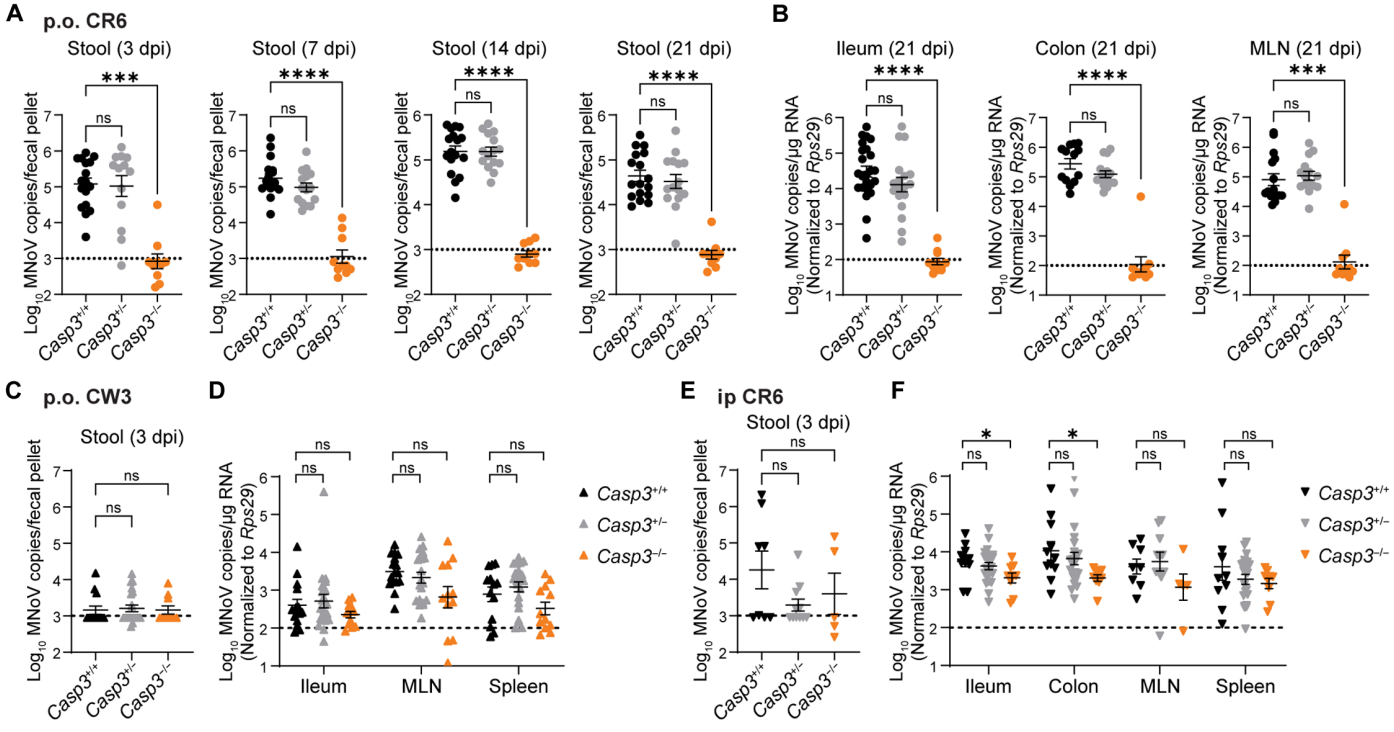


**Fig. 1. Caspase-3 is essential for MNoV intestinal infection.** (**A** and **B**) *Casp3*$^{+/+}$, *Casp3*$^{+/-}$, and *Casp3*$^{-/-}$ mice were infected with $10^6$ plaque-forming units (PFUs) of MNoV CR6 perorally (p.o.). MNoV genomes in stool at 3, 7, 14, and 21 dpi (A) and in ileum, colon, and MLN at 21 dpi (B) were quantified by quantitative reverse transcription polymerase chain reaction (qRT-PCR) ($n = 10$ to 17 mice per group, combined from three independent experiments). (**C** and **D**) *Casp3*$^{+/+}$, *Casp3*$^{+/-}$, and *Casp3*$^{-/-}$ mice were infected with $10^6$ PFU of MNoV CW3 perorally and analyzed at 3 dpi. MNoV genomes in stool (C) and in ileum, MLN, and spleen (D) were quantified by qRT-PCR ($n = 10$ to 22 mice per group, combined from three independent experiments). (**E** and **F**) *Casp3*$^{+/+}$, *Casp3*$^{+/-}$, and *Casp3*$^{-/-}$ mice were infected with $10^6$ PFU of CR6 intraperitoneally (ip) and analyzed at 3 dpi. MNoV genomes in stool (E) and in ileum, colon, MLN, and spleen (F) were quantified by qRT-PCR ($n = 5$ to 22 mice per group, combined from three or four independent experiments). Data represent means ± SEM. Data were analyzed by one-way analysis of variance (ANOVA) with Kruskal-Wallis test. ns, not significant; *$P < 0.05$; ***$P < 0.001$; ****$P < 0.0001$. The dashed lines represent the limit of detection.

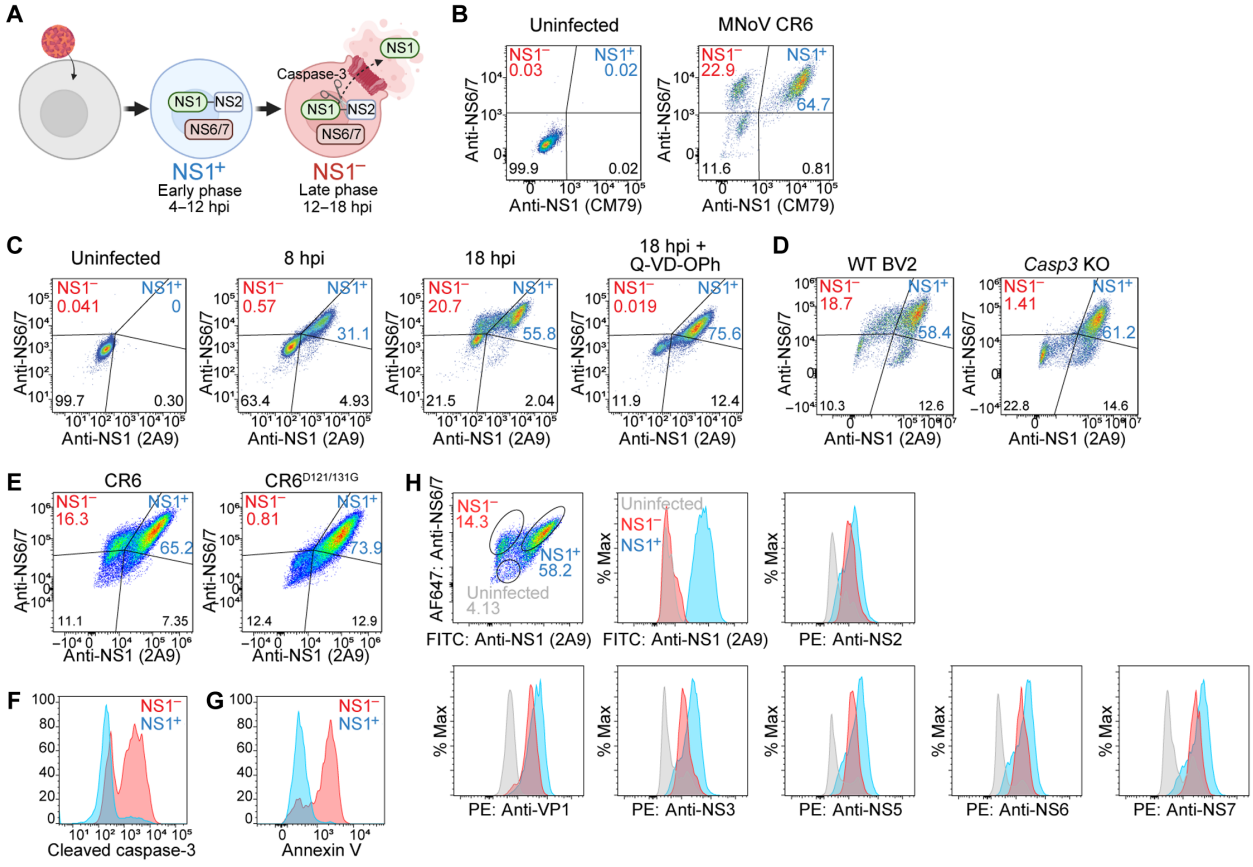


**Fig. 2. Characterization of the NS1⁻ population during MNoV infection.** (**A**) Depiction of the NS1 positivity and negativity in CR6-infected BV2 cells. (**B**) Intracellular flow cytometry plots of CR6-infected BV2 cells costained with NS6/7 and NS1 (measured with clone CM79) at 16 hpi. (**C**) Intracellular flow cytometry plots of CR6-infected BV2 cells costained with NS6/7 and NS1 (measured with clone 2A9) at 8 or 18 hpi. Q-VD-OPh (20 μM) was added along with the virus when indicated. (**D** and **E**) Intracellular flow cytometry plots of WT or *Casp3* KO BV2 cells infected with CR6 (D) or BV2 cells infected with WT CR6 or CR6$^{D121/131G}$ mutant virus (E) and costained with NS6/7 and NS1 at 18 hpi. (**F**) Comparison of caspase-3 activation in NS1⁻ and NS1⁺ cells, measured with an antibody targeting cleaved caspase-3. (**G**) Surface staining with annexin V compared in NS1⁻ and NS1⁺ cells. (**H**) BV2 cells were infected with CR6, harvested at 18 hpi, and costained with NS1, NS6/7, and other viral proteins. Intracellular levels of indicated viral proteins measured by flow cytometry in NS1⁻ and NS1⁺ cells are shown.

(NS1⁻ hereafter) cells appeared (Fig. 2C). Staining of the NS1⁻ cell population was confirmed using two anti-NS1 monoclonal clones CM79 and 2A9, which recognize different epitopes at the N-terminal sequence of NS1, detecting both NS1 and NS1/2 proteins (Fig. 2, B and C, and fig. S2, A to C). This NS1⁻ population disappeared with inhibition of caspase-3 by treatment with the pan-caspase inhibitor, Q-VD-OPh, in WT BV2 cells (Fig. 2C), infection of CR6 in *Casp3* KO BV2 cells (Fig. 2D), or infection with NS1-cleavage mutant CR6$^{D121/131G}$ (Fig. 2E). We confirmed the reduced activation of caspase-3 by Q-VD-OPh treatment or CR6$^{D121/131G}$ infection, consistent with a previous report (fig. S2D) (*30*). Most of the NS1⁻ cell population exhibited depolarized plasma membrane (annexin V positive) and activated cleaved caspase-3. In contrast, most NS1⁺ cells had intact plasma membrane without depolarization and showed minimal caspase-3 activation (Fig. 2, F and G). The NS1⁻ population exhibited a moderate loss of NS2, viral major capsid VP1, and other nonstructural proteins (Fig. 2H). Plasma membrane depolarization (annexin V positivity) and disintegration (LIVE/DEAD positivity and LDH release) were observed at similar kinetics as NS1 release (fig. S2, E to G). These results indicate that the NS1⁻ population represents the cells that have expelled all NS1 proteins outside of the cells at the late phase of viral infection with the activation of apoptosis. It strongly suggests that secretion of NS1 is a tightly controlled event given the robust, specific release of NS1, which depletes all detectable NS1, while the NS1⁻ cells largely preserve other viral nonstructural proteins and the capsid protein.

## Secretion of NS1 during MNoV infection is mediated by NINJ1

The flow cytometry assay for the NS1⁻ population provided a suitable system for unbiased screening. We conducted a genome-wide CRISPR KO screen using the BV2 CRISPR library cell line, transduced with a pool of single-guide RNAs (sgRNAs) (*31*). Cells were infected with MNoV and sorted by NS1 positivity. Comparative analysis of the CRISPR results between NS1⁻ and NS1⁺ populations identified key apoptosis genes, including *Casp3*, *Casp9*, *Apaf1*, and *Cycs* (Cytochrome C), as the top hits (Fig. 3A and table S1). Notably, *Ninj1* emerged as one of the top hits. Validation experiments with sgRNA targeting each candidate gene in polyclonal BV2 cells confirmed that the four apoptosome factors (*Casp3*, *Casp9*, *Apaf1*, and *Cycs*) and *Ninj1* are essential for the production of secreted NS1 (fig. S3, A to C). We observed a mild reduction of NS1 production and minor differences in other death markers in *Tgif1* and *Samd1* KO

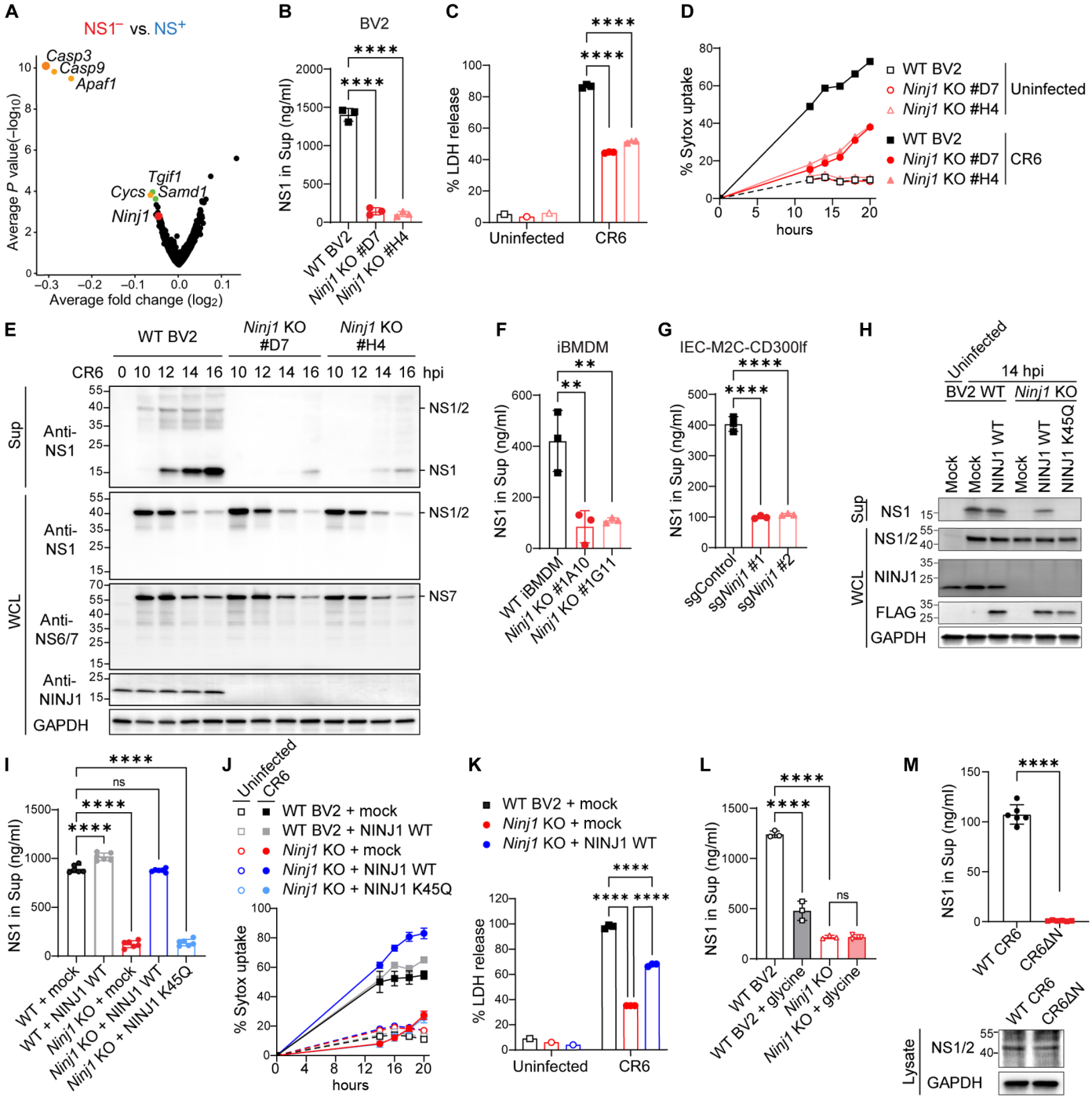


**Fig. 3. NINJ1-mediated membrane rupture is essential for NS1 secretion.** (**A**) Volcano plot showing sgRNAs depleted or enriched in NS1$^-$ cells compared to NS1$^+$ cells. (**B** to **E**) WT or *Ninj1* clonal KO BV2 cells were infected with MNoV CR6 at 5 multiplicity of infection (MOI). (B) NS1 protein levels in the supernatant were measured at 14 hpi by enzyme-linked immunosorbent assay (ELISA) ($n = 3$). (C) LDH release was measured at 16 hpi ($n = 3$). (D) Sytox uptake was measured at 12 ~ 20 hpi ($n = 3$). (E) Cells (WCL) and supernatants (Sup) were analyzed by immunoblotting at 10 ~ 16 hpi. (**F** and **G**) WT or *Ninj1* KO iBMDMs (F) or IEC-M2C-CD300lf cells transduced with indicated sgRNAs (G) were infected with CR6, and NS1 secretion was measured at 14 hpi ($n = 3$). (**H** to **K**) WT or *Ninj1* KO BV2 cells were transduced with NINJ1 WT or oligomerization-defective mutant (K45Q) and infected with CR6. (H) Cells and supernatants were analyzed by immunoblotting at 14 hpi. (I) NS1 secretion was measured by ELISA at 14 hpi ($n = 6$). (J) Sytox uptake was measured at 14 ~ 20 hpi ($n = 3$). (K) LDH release was measured at 16 hpi ($n = 3$). (**L**) WT or *Ninj1* KO BV2 cells were infected with CR6 and treated with glycine (5 mM). NS1 secretion was measured at 14 hpi ($n = 3$). (**M**) BV2 cells were infected at 1 MOI with WT CR6 or mutant virus (CR6ΔN) and analyzed by ELISA and immunoblotting at 10 hpi ($n = 6$ from two independent experiments). Data represent means ± SEM. Data were normalized to Tween-20–treated control [(C), (D), (J), and (K)]. Data were analyzed by one-way ANOVA with Dunnett's multiple comparisons test [(B), (C), (F), (G), and (I)] and Tukey's multiple comparisons test [(K) and (L)] or two-tailed unpaired Mann-Whitney test (M). ns, not significant; $^{**}P < 0.01$; $^{****}P < 0.0001$. Data are representative of three independent experiments.

BV2 cells (fig. S3, D to G). Most strikingly, genetic ablation of *Ninj1* in clonal BV2 cells abolished secretion of NS1, release of LDH, and plasma membrane permeabilization during MNoV CR6 infection (Fig. 3, B to D). Immunoblotting using an anti-NS1 monoclonal antibody confirmed that cleaved NS1 protein is exclusively detected in the culture supernatant in contrast to the abundant intracellular expression of the precursor protein NS1/2 (Fig. 3E). Secretion of NS1 was abolished in *Ninj1* KO cells, while intracellular expression of NS1/2 and NS7 was not largely affected (Fig. 3E).

To investigate the release of cellular DAMPs and viral proteins via NINJ1 during MNoV infection, we conducted a secretome analysis by bulk mass spectrometry (MS). In WT and *Ninj1* KO BV2 cells, the landscape of proteins released into the culture supernatant was analyzed with human immunoglobulin G (IgG) used as a spike-in control for normalization. This analysis revealed that more than 2000 cellular proteins, including DAMPS (e.g., LDH, HMGB1, and histones), were released from WT BV2 cells but were largely depleted in the culture supernatant from *Ninj1* KO cells (fig. S3, H and I, and table S2). Viral proteins including NS1 and virion proteins [VP1, VP2, and NS5 (VPg)] were abundantly detected in WT cells as expected and their release was depleted in *Ninj1* KO cells, consistent with previous findings that demonstrated NINJ1-dependent egress of MNoV virions (fig. S3J) (*10*). In addition to NS1, the release of two other nonstructural proteins, NS6 and NS7, was also identified (fig. S3K). We further examined the intracellular and extracellular ratios of individual nonstructural proteins by immunoblot. NS1 was exclusively detected in the supernatant, while the NS1/2 precursor, NS2, and NS3 were solely detected in the cell lysate. NS5 (VPg) and NS7 were present in both the supernatant and the lysate in comparable amounts (fig. S3L). This pattern of intra/extracellular ratio aligns with the observed complete loss of NS1 and partial loss of other intracellular nonstructural proteins in the $NS1^-$ population by flow cytometry (Fig. 2H). Collectively, the secretome analysis demonstrates the bulk release of a milieu of cellular DAMPs and viral virions and nonstructural proteins, along with the effective and robust release of NS1 during MNoV infection, which is largely dependent on NINJ1.

Since the release of NS6 and NS7 in BV2 cells was observed, we questioned which viral nonstructural proteins elicit antibody responses upon peroral CR6 infection in mice. While VP1 and NS1 induced robust antibody responses, no detectable antibody responses were observed against NS2 or NS6/7 (fig. S3M). These findings suggest that secreted NS1 is sufficient to elicit anti-NS1 responses during natural MNoV infection. Given the absence of seroconversion for NS6 and NS7, it is likely that these proteins are either not released in vivo or are released at levels not physiologically relevant to trigger an antibody response.

The role of NINJ1 in NS1 secretion was confirmed in two other MNoV-susceptible cells, including immortalized bone marrow–derived macrophages (iBMDM) and the mouse intestinal epithelial line M2C-CD300lf (Fig. 2, F and G, and fig. S4, A to C). Release of NS1 during acute MNoV (CW3) infection was also dependent on NINJ1 in these cells (fig. S4D). In addition, *Ninj1* depletion in these cells resulted in defects in Sytox uptake and LDH release in response to apoptotic or pyroptotic stimuli (fig. S4, E to H). *Ninj1* KO BV2 cells showed a comparable caspase-3 activation during MNoV infection, suggesting that the defective secretion of NS1 in *Ninj1* KO cells is a downstream event after caspase-3 activation (fig. S4I). While NS1 secretion is abolished in *Casp3* KO BV2 cells, Sytox uptake and release of LDH were less altered compared to *Ninj1* depletion, indicating that NS1 cleavage by caspase-3 and the plasma membrane rupture are not interdependent within the infected cells (fig. S4, J and K).

Multiple studies have shown cross-regulation and redundant function of caspases in different cell death pathways. Gasdermin family proteins are critical for the release of IL-1 family cytokines [reviewed in (*32*–*34*)]. Caspase-3 directly cleaves gasdermin E (GSDME), which leads to apoptotic and/or pyroptotic cell death and release of IL-1 cytokines (*35*, *36*). The CRISPR screening result did not implicate gasdermins or other caspases in NS1 secretion (Fig. 3A). We confirmed that knocking out gasdermins or caspases, except *Casp3*, *Casp9*, and partially *Casp7*, did not alter NS1 secretion (fig. S5, A and B). To rule out the function of GSDMD and GSDME, a *Gsdmd/Gsdme* double KO (DKO) BV2 clone was generated (fig. S5, C and D). The DKO clonal BV2 cells retained all indicators: secretion of NS1, the $NS1^-$ population by flow cytometry, LDH release, and Sytox uptake upon MNoV infection despite the defects in reacting to the pyroptotic stimulus (fig. S5, E to H). Collectively, secretion of NS1 is dependent on the apoptosome-NINJ1–mediated process rather than gasdermin pores.

Osmotic swelling and permeabilization of the plasma membrane are features of the execution phase of apoptosis. The late phase of MNoV infection in BV2 cells exhibited features of apoptosis execution, including osmotic swelling and permeabilization of the plasma membrane. *Ninj1* KO cells displayed a distinct phenotype, remaining intact plasma membrane without permeabilization, with many cells exhibiting highly swollen apoptotic bodies. This pattern was also observed with the control apoptotic stimulus, etoposide (fig. S5I).

Self-oligomerization of NINJ1 was found to be crucial for executing plasma membrane rupture in swollen, dying cells (*1*). To characterize the features of virally induced death, the *Ninj1* KO BV2 clone was complemented by ectopic expression of WT NINJ1 or a nonfunctional form of NINJ1 [K45Q and A59P, defects in self-oligomerization (*1*)]. Using a native polyacrylamide gel electrophoresis (PAGE) experiment, we found that MNoV infection induced oligomerization of NINJ1, which is comparable to the positive control stimulus, etoposide (fig. S5J). Complemented expression of WT NINJ1 rescued secretion of NS1, Sytox uptake, the $NS1^-$ population in flow cytometry, while the oligomerization-defective NINJ1 with K45Q mutation did not (Fig. 3, H to J, and fig. S5, J and K). Release of a cellular DAMP marker, LDH, was substantially reduced in *Ninj1* KO cells and recovered by the NINJ1 complementation (Fig. 3K). In addition, chemical inhibition of plasma membrane rupture by glycine in the culture medium strongly suppressed NS1 secretion during infection, further supporting the importance of the membrane rupture in this process (Fig. 3L and fig. S5L) (*37*, *38*). Overexpression of caspase-3 showed no effect on membrane permeability or NS1 secretion in *Ninj1* KO cells, confirming caspase-3 functions at upstream of NINJ1 (fig. S5, M and N).

MNoV NS3 protein is recently reported to activate caspase-3 through mitochondrial permeabilization and cytochrome C release during infection (*10*). In alignment with this, a mutant MNoV CR6 harboring an N-terminal domain deletion of NS3 (CR6ΔN) (*10*) lost its ability to produce secreted NS1, while intracellular NS1/2 precursor levels remained unchanged (Fig. 3M). This suggests that MNoV NS3–triggered apoptosis leads to NINJ1-mediated execution of membrane rupture, resulting in the release of NS1.

### NINJ1-mediated secretion of NS1 is a selective process with specificity

In an infection-free transfection model, we observed that ectopic overexpression of StrepTag-NS1/2 in BV2 cells was sufficient to

induce cleavage and secretion of NS1 with the moderate activation of caspase-3 (Fig. 4, A and B), consistent with previous reports (*5*, *10*, *30*). We validated that StrepTag-NS1 secretion was dependent on *Ninj1* expression (Fig. 4C). This infection-free model allowed us to elucidate the molecular requirements for the selective release of NS1. Two different approaches were used. Truncation of the N-terminal amino acids 1 to 47 of NS1 was dispensable for protein secretion, while truncation of amino acids 48 to 74 was crucial for secretion (Fig. 4D). A triple-alanine scanning approach identified four critical regions required for NS1 secretion: One in the unstructured region and three in the helix-strand-helix (HSH) motif (Fig. 4, A and E). A construct with the cleavage mutations (D121/131G) was used as a positive control. The four identified regions were further validated at the single–amino acid level to minimize structural disruption of the HSH motif by preserving the secretion defect. This point mutagenesis study specified five key residues (P73, L99, D100, Y110, and H112) for NS1 secretion, most of which are located in non-helical regions (*39*) (Fig. 4, F and G).

To investigate the specificity of protein secretion, we examined the differential secretion of NS1 WT and NS1 mutants with secretion-defective mutations when coexpressed. BV2 cells with either NS1 WT or the P73L mutation using an inducible Tet-on lentiviral system were established for moderate gene expression. BV2 cells were infected with MNoV, followed by induction of StrepTag-NS1/2 expression. The P73L mutant exhibited a specific defect in its secretion after cleavage while endogenous viral NS1 was effectively secreted (Fig. 4H). Of note, cleaved StrepTag-NS1 accumulated intracellularly for the secretion-defective clone. Release of LDH was not affected in these cells, pinpointing the specific defect in secretion of the P73L mutant (Fig. 4I). Together, these results indicate that NS1 release from dying cells is selectively controlled, suggesting that specific amino acid residues in NS1 dictate the "go or no-go" decision for specific secretion via NINJ1 when membrane-ruptured cells bulk-release intracellular proteins.

### NS1 interaction with NINJ1 mediates NS1 release

To gain mechanistic insight into the NINJ1-mediated specific secretion of NS1, we performed a series of cellular and biochemical assays. Coimmunoprecipitation indicated that NINJ1 interacts with NS1 and/or NS1/2 in cells during MNoV infection (Fig. 5A). To determine the subcellular localization of NINJ1 and NS1, we used the *Ninj1* KO BV2 cells complemented with Flag-NINJ1 WT ectopic expression. This construct rescues the functional defects in secretion of NS1 and the DAMPs (as shown in Fig. 3). This cell line model was subjected to immunogold transmission electron microscopy to characterize the cytoplasmic features at ultrastructural resolution. NINJ1 clustered close to the plasma membrane and ER membranes in uninfected cells (Fig. 5B and fig. S6A). During MNoV infection, NINJ1 was detected in vesicle-like double-membraned structures resembling the viral replication complex, with several NINJ1 points in close proximity to NS1 staining on the membrane of the viral replication factory (Fig. 5C and fig. S6B). These vesicle structures shared the reported features of viral replication complex, which contained virus within single- or double-membraned vesicles in the cytoplasm (*15*, *40*). Such colocalization of NS1 and NINJ1 was observed at a later time point as well where subcellular structures and membranes are compromised (fig. S6C). The nonfunctional mutant NINJ1 (K45Q) showed similar localization to WT NINJ1, suggesting that NINJ1 oligomerization is not required for its recruitment to the viral replication complex (fig. S6, D to F). Confocal immunofluorescence assay confirmed colocalization of NINJ1 and NS1 in intracellular foci during MNoV replication (Fig. 5D and fig. S7B). In uninfected cells, NINJ1 exhibited a dispersed intracellular localization throughout plasma membrane and ER-looking localization and similar pattern was observed after MNoV infection (fig. S7A). However, staining of NINJ1 started showing speckled patterns at 10 ~ 14 hpi but not with K45Q mutation, likely depending on NINJ1 oligomerization (Fig. 5D and fig. S7A). More than 20% of these NINJ1 speckles colocalized with NS1 (Fig. 5, D and E). These overlapping foci with NINJ1 and NS1 were also positive for NS6/7 staining. In addition, treatment of the pan-caspase inhibitor Q-VD-OPh did not interrupt the colocalization (fig. S7A), suggesting that the colocalization occurred at the viral replication complex and was not dependent on liberating NS1 by caspase-cleavage. During MNoV infection, NINJ1 speckles localized to the ER and endosome along with NS1 costained at the foci (fig. S7, C and D).

A binding enzyme-linked immunosorbent assay (ELISA) demonstrated the direct interaction between recombinant NS1 and Fc-tagged ectodomain of human or mouse NINJ1 with an affinity comparable to a monoclonal NS1 antibody (Fig. 5F). Recombinant human and mouse NINJ1 proteins with a His-tag, but not a negative control protein LRRC15 ectodomain (*41*), also showed comparable affinities for NS1 binding (fig. S7, E to G). We validated the binding of mouse NINJ1 ectodomain to NS1 using microscale thermophoresis (MST). Deletion of the α2 helix in NINJ1 abolished the binding to NS1, whereas mutations in amino acids critical for oligomerization or deletion of the α1 helix had no effect (Fig. 5G). Further analysis revealed that the C-terminal region of NS1 (65-121) is essential for binding to NINJ1, which contains key amino acid residues necessary for NS1 secretion (Fig. 5H). Notably, NS1 proteins with triple-alanine mutations in the C-terminal region lost interaction with NINJ1, while both WT and mutant NS1 proteins retained binding affinity to the control protein, anti-NS1 CM79, which targets the N-terminal epitope (1–31) of NS1 (Fig. 5, H and I). These findings collectively support the conclusion that NS1 directly interacts with NINJ1 during MNoV infection and that this interaction is required for the specific secretion of NS1 protein.

Phosphoinositides (phosphatidylinositol phosphates, PIPs) have been implicated in the regulation of programmed cell death by serving as trafficking platforms for membrane proteins, directing them to subcellular lipid membrane organelles (*42*–*44*). Recent studies have highlighted the role of phosphoinositide in gasdermin pore formation and their potential impact on membrane rupture (*45*–*48*). We investigated the potential utilization of phosphoinositides by NS1 for controlled release. Initially, we generated recombinant NS1 proteins with a His-tag and assessed the lipid-binding affinity of NS1 using a membrane lipid strip. Intriguingly, NS1 exhibited substantial affinity for multiple phospholipids, with higher affinity observed for PI(3)P and PI(5)P, and moderate affinity for PI(4)P and PI(3,5)$P_2$ (fig. S7H). His-NS1 protein with an N-terminal truncation (His-$NS1^{65–121}$) exhibited a partial loss of binding affinity, while the triple-alanine mutations showed comparable binding affinities (fig. S7, I and J). These findings suggest that the N-terminal region of NS1 plays a role in phosphoinositide binding. The binding affinity to PI(3)P and PI(5)P was further validated by isothermal titration calorimetry (ITC), revealing moderate affinities for these phospholipids (fig. S7K). PI(3)P is known to be present at the plasma membrane and within the endosome (*49*). Similarly, PI (5)P has been reported to localize to the

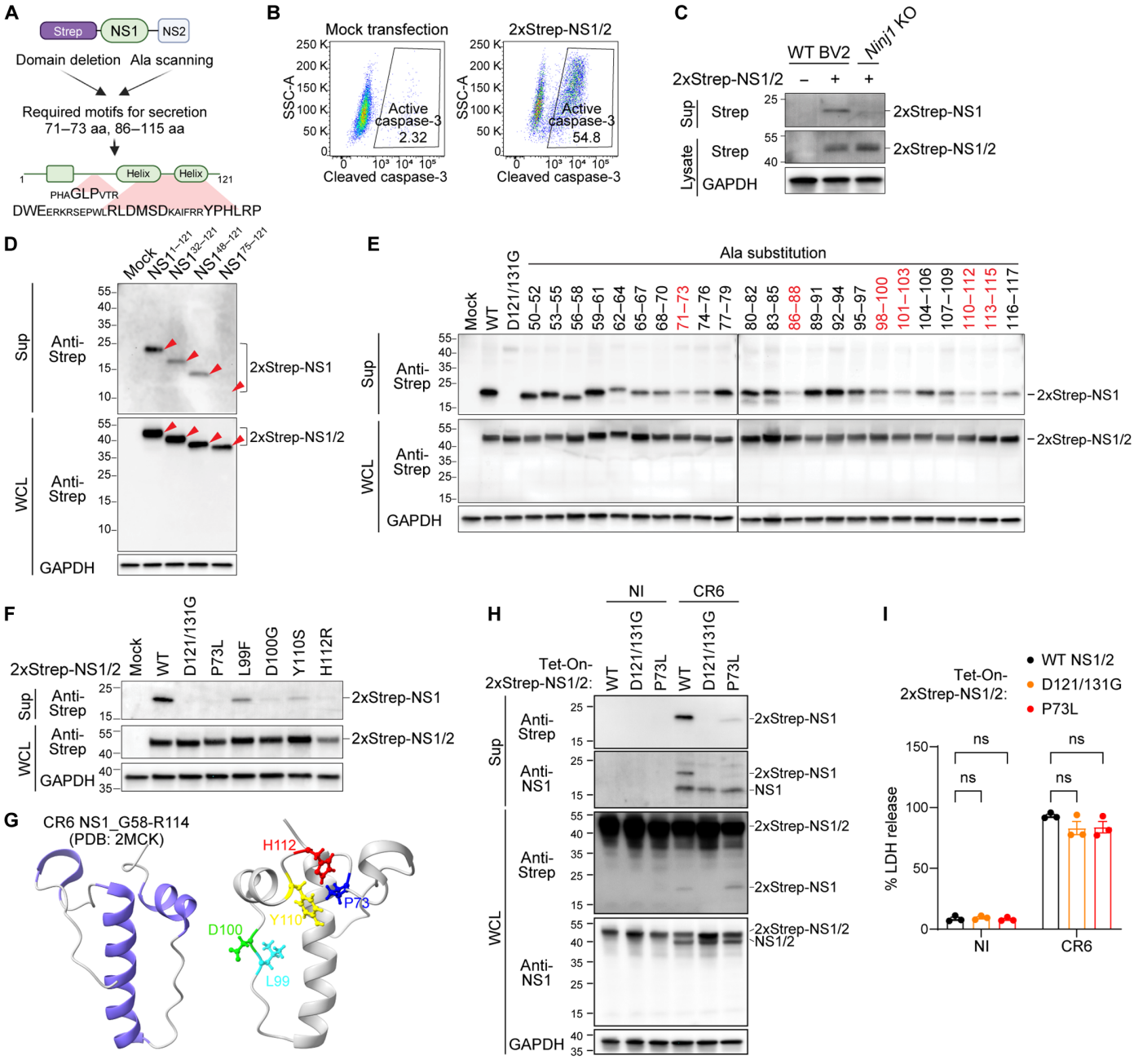


**Fig. 4. Amino acid residues within NS1 required for the specific secretion of NS1.** (**A**) Mutant studies revealed residues required for NS1 secretion. (**B**) BV2 cells were transfected with a mock vector or 2xStrep-NS1/2 and caspase-3 activation was measured by flow cytometry. (**C**) WT or *Ninj1* KO BV2 cells were transfected with 2xStrep-NS1/2. Cells and supernatants were harvested at 24 hours posttransfection and analyzed by immunoblotting. (**D**) BV2 cells were transfected with 2xStrep-tagged NS1/2 constructs with N-terminal truncation mutations, and cells and supernatants were analyzed by immunoblotting at 24 hours posttransfection. Red arrowheads indicate different truncation mutants. (**E**) BV2 cells were transfected with D121/131G cleavage mutant and triple-alanine scanning mutants and analyzed as in (D). Numbers indicate amino acid residues substituted by alanine. Mutants showing defect in secretion are highlighted in red. (**F**) BV2 cells were transfected with NS1/2 constructs with indicated point mutations and analyzed as in (D). (**G**) 3D structure of CR6 NS1 (58 to 114 amino acids; PDB: 2MCK) highlighting the key residues identified from mutagenesis study. (**H** and **I**) BV2 cells with doxycycline-inducible expression of 2xStrep-tagged WT or mutant NS1/2 were infected with MNoV CR6 and incubated with doxycycline (2 μg/ml) for 12 hours. (H) Cells (WCL) and supernatants (Sup) were analyzed by immunoblotting. (I) LDH release was measured and normalized to Tween-20–treated control ($n = 3$). Data represent means ± SEM and were analyzed by two-way ANOVA with Dunnett's multiple comparisons test.

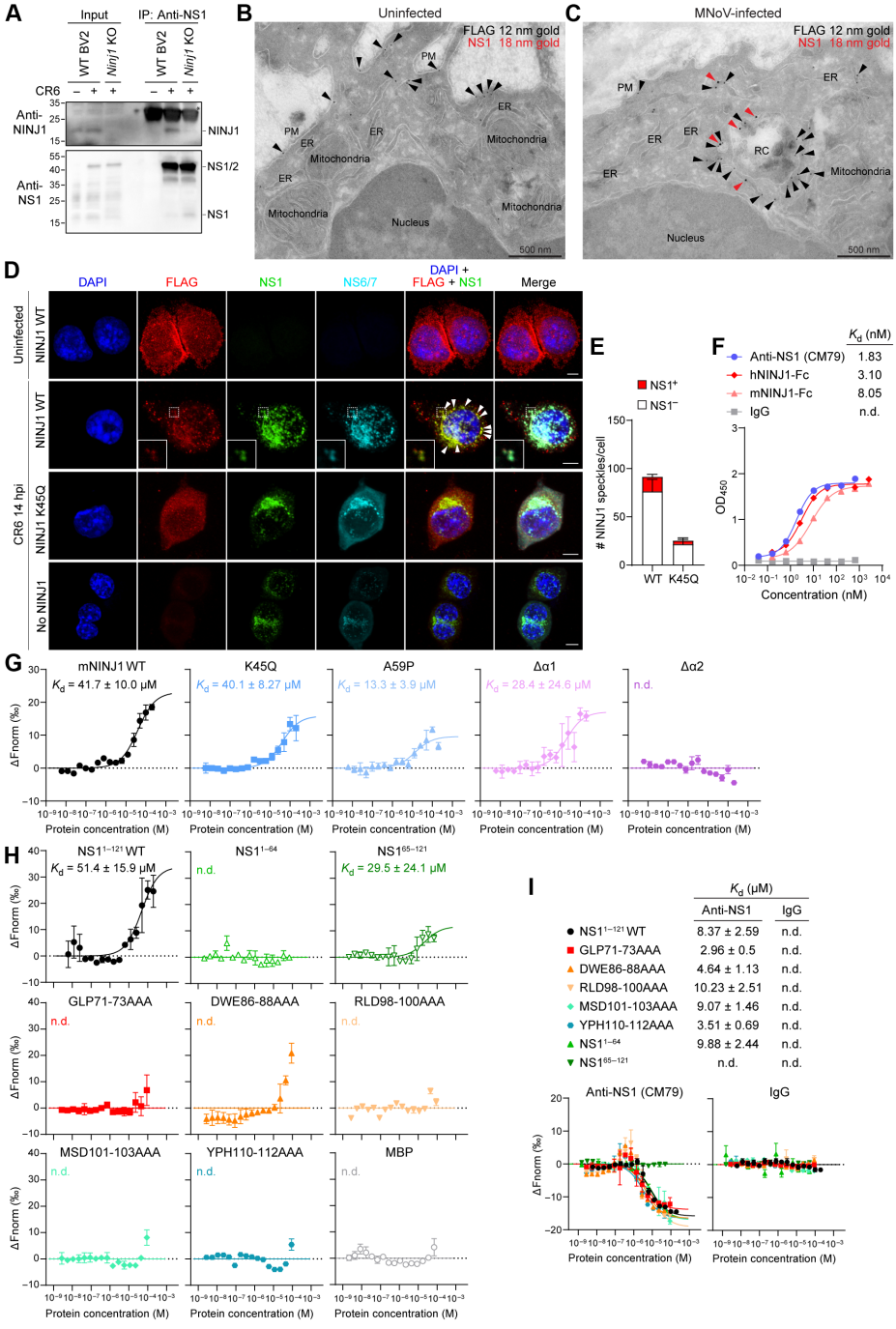


**Fig. 5. NS1 directly binds to NINJ1.** (**A**) WT or *Ninj1* KO BV2 cells were infected with CR6 at 5 MOI and harvested at 10 hpi. Cell lysates were immunoprecipitated with anti-NS1 and analyzed by immunoblotting. (**B** and **C**) Transmission electron microscopy image of uninfected (B) or CR6-infected (C) BV2 cells with immunogold labeling for FLAG-NINJ1 (12-nm gold, black arrowheads) and NS1 (18-nm gold, red arrowheads). RC, replication complex. Scale bar, 500 nm. (**D**) Representative immunofluorescence confocal imaging of FLAG-NINJ1 (red), NS1 (green), NS6/7 (cyan), and 4′,6-diamidino-2-phenylindole (DAPI, blue) in *Ninj1* KO BV2 cells reconstituted with FLAG-NINJ1 WT or K45Q at 14 hpi. White arrowhead highlights the colocalization of NINJ1 and NS1 proteins. Scale bars, 5 μm. All images are representative of three or more independent experiments. (**E**) Quantification of colocalization between NS1 and FLAG-NINJ1 WT or K45Q. Bars represent means ± SEM, $n = 10$ to 11 cells. (**F**) Dose-dependent binding of Fc-tagged ectodomain of human NINJ1 (hNINJ1) or mouse NINJ1 (mNINJ1) protein to recombinant NS1 protein was determined by ELISA. A monoclonal anti-NS1 (clone CM79) and isotype control were included as a positive and negative control, respectively. Data represent means ± SEM of duplicates, and the dissociation constants ($K_d$) are shown. (**G** to **I**) Direct binding between recombinant NS1 and mNINJ1 protein was measured by MST. ΔFnorm indicates the change in thermophoresis, and $K_d$ is shown. n.d., not determined. (G) Dose-response curve showing bindings of WT NS1 protein to fluorescence-labeled WT or mutated mNINJ1 proteins. (H) Dose-response curve showing bindings of WT or mutated NS1 proteins to fluorescence-labeled mNINJ1. Maltose-binding protein (MBP) was included as a negative control. (I) Dose-response curve showing bindings of WT or mutated NS1 proteins to fluorescence-labeled monoclonal anti-NS1 or isotype control. Data are shown in means ± SEM ($n = 3$).

plasma membrane, early endosomes, and the nucleus (*50*). Notably, a recent study demonstrated NINJ1 binding to PI(4)P and its incorporation into PI(4)P-containing liposomes in vitro (*4*). While the role of phosphoinositides in norovirus infection remains unexplored, our results underscore their potential involvement in the formation of the viral replication complex, NINJ1 recruitment, or the initiation of plasma membrane rupture.

### HSP90 plays a crucial role in MNoV-mediated caspase-3 activation and viral infection in mice

Genetic studies have demonstrated that the ablation of caspase-3 renders mice resistant to peroral MNoV CR6 (Fig. 1). The oral CR6 infection model mimics fecal-oral human norovirus (HNoV) transmission, representing the natural infection route of norovirus. This prompted us to conduct a drug screening using a Food and Drug Administration (FDA)–approved drug library, encompassing 2321 individual drugs, to investigate whether the secretion of NS1 during norovirus infection could be a druggable target. BV2 cells were infected with MNoV CR6 in the presence of drug, and secreted NS1 was quantified by sandwich ELISA (Fig. 6A). The primary screen identified 65 drugs that inhibited more than 50% of the secreted NS1 amount in two biological repeats, segregating them into two phenotypic groups. The first group consisted of drugs inhibiting viral entry/replication, with a completely abolished viral replication (fig. S8, A to C). For instance, tubulin inhibitors, such as vinblastine and vinorelbine, were effective in inhibiting viral replication, likely by blocking viral protein trafficking to form replication complex (fig. S8, D to G) (*51*). In the second group, a subset of heat-shock protein 90 (HSP90) inhibitors, including 17-AAG, AT13385, and ganetespib, strongly suppressed NS1 production in BV2 (Fig. 6, A

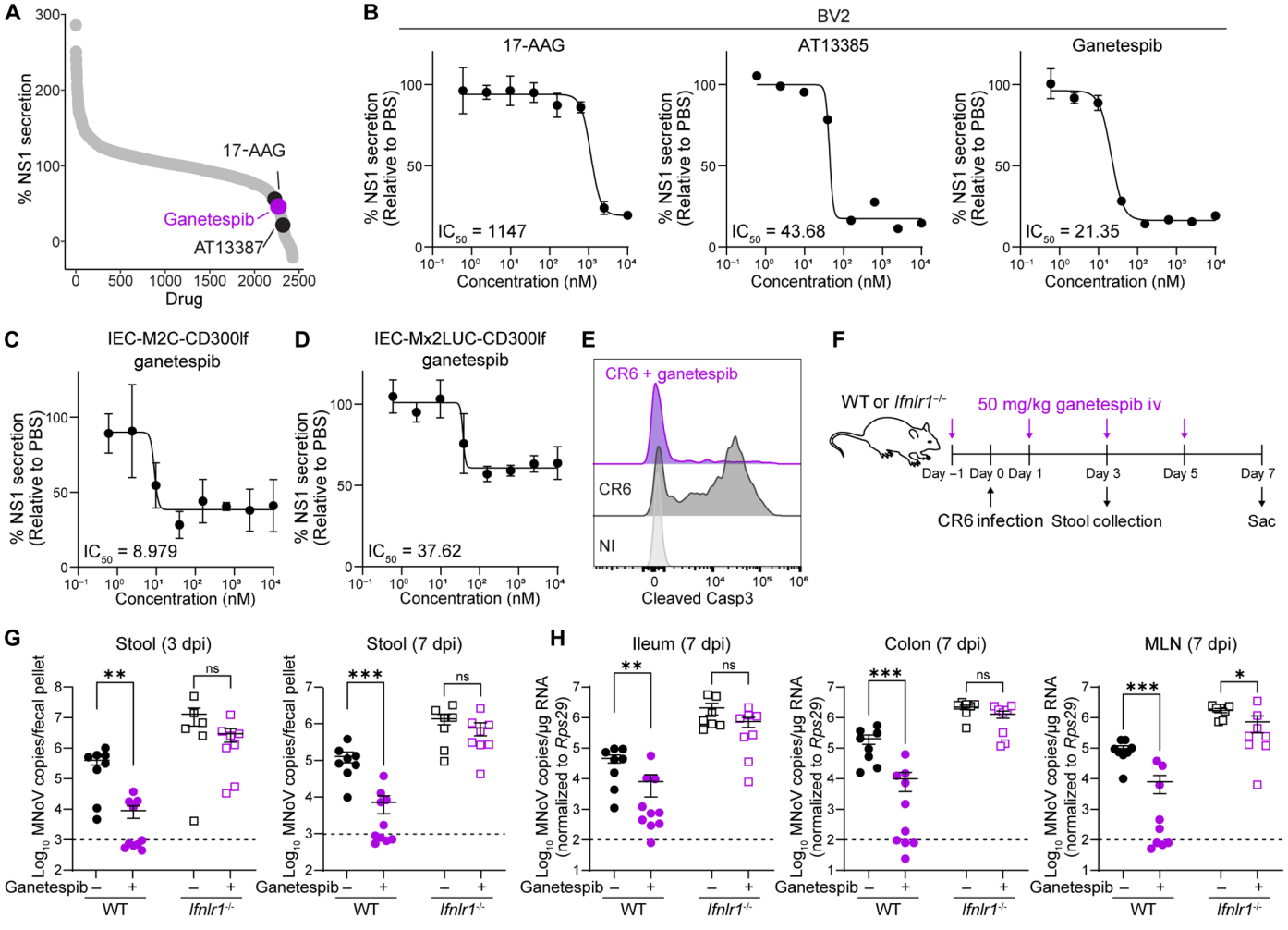


**Fig. 6. HSP90 inhibitors prevent NS1 secretion by blocking caspase-3 activation.** (**A**) BV2 cells were infected with CR6 at 5 MOI in the presence of 2321 FDA-approved drugs (dots represent individual drugs tested). NS1 levels in the supernatant were measured by ELISA at 16 hpi and normalized to vehicle control. Representative results from two independent experiments are shown. (**B** to **D**) Cells were infected with CR6 in the presence of serial dilutions of drugs. NS1 secretion was measured by ELISA at 16 hpi and normalized to no-drug control. $IC_{50}$ values (nM) determined by four biological replicates are shown. BV2 cells were treated with 17-AAG (left), AT13385 (middle), or ganetespib (right) (B). IEC-M2C-CD300lf (C) or IEC-Mx2LUC-CD300lf (D) cells were treated with ganetespib. (**E**) Caspase-3 activation in CR6-infected BV2 cells with ganetespib (10 μM) was measured with an antibody targeting cleaved caspase-3. For (B) to (E), data are representative of two to three independent experiments. (**F** to **H**) WT or *Ifnlr1*$^{-/-}$ B6 mice were infected with $10^6$ PFU CR6 perorally. Ganetespib was given intravenously (50 mg/kg, iv) as experimental treatment scheme (F). MNoV genomes in stool (G), ileum, colon, and MLN (H) at indicated time points were quantified by qRT-PCR ($n = 7$ to 10 mice per group, combined from two independent experiments). Data represent means ± SEM and analyzed by two-tailed unpaired Mann-Whitney test. ns, not significant; *$P < 0.05$; **$P < 0.01$; ***$P < 0.001$.

and B). This inhibition was confirmed in two MNoV-susceptible mouse intestinal epithelial lines, IEC-M2C-CD300lf and IEC-Mx2LUC-CD300lf (Fig. 6, C and D). Intriguingly, the inhibition of NS1 production was observed while preserving the expression of NS1/2 and NS6/7 and permitting execution of death of infected cells with release of other cellular DAMPs and permeabilization of the plasma membrane (fig. S8, H to J). Notably, ganetespib completely abolished the activation of caspase-3 during MNoV infection (Fig. 6E). The inhibitory effect of ganetespib was also observed upon cell-intrinsic stimulus, etoposide. Cells treated with ganetespib were protected from membrane permeabilization or caspase-3 activation (fig. S8, K and L). Together, these results indicate that the inhibition of HSP90 specifically targets NS1 production by blocking caspase-3 activation with minimal effects on virus-induced cell death.

Ganetespib treatment reduced VP1 capsid protein expression and production of infectious viral particles (fig. S8, M and N), consistent with a previous report (*52*). The HSP90 inhibitor 17-DMAG exhibited approximately a one-log reduction in viral titer during acute CW3 infection in WT mice (*52*). This led to our hypothesis that HSP90 inhibitors could offer a previously unknown therapeutic avenue for oral norovirus infection, particularly considering their dual impact on caspase-3 activation and regulation of capsid expression. To test this, WT mice were intravenously injected with ganetespib at a relevant dose for human treatment (50 mg/kg) (Fig. 6F) (*53*). Ganetespib treatment effectively suppressed oral infection of MNoV CR6, as indicated by substantially reduced viral shedding into the stool and diminished viral titers in intestinal tissues and lymph nodes (Fig. 6, G and H). Intriguingly, this effective viral suppression was contingent on intact IFN-λ host immunity, as the inhibitory effect was largely mitigated in IFN-λ receptor–deficient (*Ifnlr1*$^{-/-}$) animals (Fig. 6, G and H). Together, the HSP90 inhibitor plays a crucial role in suppressing viral challenges at the intestinal mucosal site, exerting a synergistic antiviral effect by making it more susceptible to host IFN-λ immune responses (as demonstrated in this study) and by destabilizing viral capsid proteins [as referenced in (*52*)]. These results provide insights into host-directed therapy by targeting viral immune evasion molecules and enhancing host immune control against viral infections. Our drug screen revealed that another drug, quizartinib (an antagonist for FLT3, fms-like tyrosine kinase 3), effectively prevented NS1 secretion by inhibiting caspase-3 activation. Unlike the HSP90 inhibitors, quizartinib treatment did not affect the VP1 capsid expression (fig. S8, H and N to P), suggesting that virally induced apoptosis could be an important therapeutic target for MNoV treatment, independent from viral capsid regulation.

## DISCUSSION

This study elucidates the co-option of NINJ1 for protein secretion, representing a previously unidentified instance of a noncellular protein using this pathway for controlled, specific release (fig. S8Q). Contrary to previous views (*1*–*3*), our findings suggest that the release of intracellular NS1 via NINJ1 is not determined by size or solubility. First, NS1, the small viral protein (~15 kD), challenges the size-dependency hypothesis. Second, specific amino acid residues of NS1 play a decisive role in the go or no-go decision for secretion through its interaction with NINJ1. While NINJ1 triggers plasma membrane rupture and bulk-release of intracellular DAMPs, NINJ1 simultaneously serves as a highly effective secretion platform for NS1.

Results in this study indicate that NINJ1-mediated plasma membrane rupture, at least for NS1 secretion, functions as a precisely regulated, specific cellular mechanism for releasing intracellular proteins, distinguishing it from the nonspecific, bulk release of cellular DAMPs and virions. Current models suggest that NINJ1 oligomerization may lead to membrane rupture either by pore formation or by the release of lipid nanodisks (*3*, *4*). NS1 may be secreted alongside these events, potentially along with the release of cellular DAMPs. Alternatively, it is plausible that NS1 secretion occurs via a different mechanism than DAMPs (*54*–*56*). Given the membrane-associated nature of the NS1/2 protein and NS1's binding affinity to PIP lipids, it is possible that NINJ1 is recruited to the viral replication complex, traffics to the plasma membrane with NS1, and serves as a protein-trafficking platform for NS1 secretion. The lipid nanodisk model and the shared PI(4)P-binding affinity between NS1 and NINJ1 may support this hypothesis. Nonetheless, the secretion of NS1 is exclusively dependent on NINJ1 through its direct interaction, highlighting NS1 as an attractive model for in-depth investigations into both the mechanistic aspects of NINJ1 and the execution phase of cellular death.

An intriguing question arises as to why NS1 co-opts NINJ1 over other unconventional or conventional secretion pathways. One possibility is that the NINJ1 pathway effectively expels all NS1 upon the activation of a death cue, as observed in the NS1$^{-}$ population. Further investigation is needed to understand whether NINJ1-mediated secretion enhances the functionality of NS1 immune evasion. The secretion of NS1 of HNoV GI.1 in an infection-free transfection model was observed (*5*), and caspase cleavage of NS1 proteins from both GI and GII genogroups of HNoV has been reported in vitro (*57*). This suggests that the maturation and secretion of NS1 via caspases and NINJ1 could be an evolutionarily conserved mechanism between human and mouse noroviruses, highlighting the therapeutic implication of targeting the apoptosis/NINJ1 pathway to disrupt norovirus infection and immune evasion. The requirement of NINJ1 for MNoV NS1 appears to be conserved across tested epithelial and myeloid cells. In conclusion, this study offers potential insights into the unexplored role of NINJ1 in controlled protein secretion, providing a foundation for further exploration of its broader implications in infectious diseases and other human diseases.

## MATERIALS AND METHODS

### Reagents and antibodies

DiscoveryProbe FDA-approved Drug Library (L1021) and individual drugs including Q-VD-OPh (A1901), 17-AAG (A4054), AT13387 (A4056), ganetespib (A4385), and quizartinib (A5793) were purchased from Apexbio. Ultrapure lipopolysaccharide (LPS) (*Escherichia coli* O111:B4, tlrl-3pelps) was purchased from Invivogen. Nigericin (N7143), etoposide (E1383), adenosine triphosphate (ATP, A2383), glycine (G8790), and trichloroacetic acid (TCA, T9159) were purchased from Sigma-Aldrich. Staurosporine (1285) was purchased from Tocris.

Primary antibodies used in this study include the following: Strep-tag II (A01732, Genscript), FLAG (for immunoblotting; 200-350-383, Rockland Immunochemicals), FLAG (for immunofluorescence; 637303, BioLegend), 6xHis (ab18184, Abcam), GSDMD (ab209845, Abcam), active caspase-3 (clone C92-605; 559565, BD Biosciences), glyceraldehyde-3-phosphate dehydrogenase (MCA4739, Bio-Rad), calnexin (ab22595, Abcam), RAB7 (ab137029, Abcam), ATP5A1

(14676-1-AP, Proteintech), and TGN46 (ab16059, Abcam). Rabbit polyclonal anti-NINJ1 (A16406, Abclonal) was used in all shown immunoblots. Staining results were confirmed by rabbit polyclonal anti-NINJ1 provided from S. H. Oh (*58*) and S. -J. Bae (*59*). Mouse monoclonal anti-NS1 (clone CM79) was provided from V. Ward. Rabbit polyclonal anti-NS3, NS5, NS6, and NS7 were provided from I. Goodfellow. Mouse monoclonal anti-VP1 (clone A6.2) was generated in our previous study (*15*). Mouse monoclonal anti-NS1 (clone 2A9), hamster monoclonal anti-NS1 (clone 11G10), rabbit polyclonal anti-NS1, rabbit polyclonal anti-NS2 (clone R697), and guinea-pig polyclonal anti-NS6/7 are generated in this study. Secondary antibodies used in this study include the following: StarBright Blue 700 goat anti-mouse IgG (12004158, Bio-Rad), StarBright Blue 700 goat anti-rabbit IgG (12004161, Bio-Rad), StarBright Blue 520 goat anti-mouse IgG (12005866, Bio-Rad), StarBright Blue 520 goat anti-rabbit IgG (12005869, Bio-Rad), goat anti-guinea pig IgG–horseradish peroxidase (HRP) (6090-05, Southern Biotech), goat anti-mouse IgG1-HRP (1071-05, Southern Biotech), goat anti-mouse IgG2b-HRP (1091-05, Southern Biotech), rabbit anti-hamster IgG-HRP (6211-05, Southern Biotech), fluorescein isothiocyanate (FITC) anti-mouse IgG1 (553443, BD), FITC anti-mouse IgG2b (406705, BioLegend), phycoerythrin (PE) anti-guinea pig IgG (706-116-148, Jackson ImmunoResearch), PE anti-rabbit IgG (711-116-152, Jackson ImmunoResearch), Alexa Fluor 647 anti-mouse IgG2a (407115, BioLegend), Alexa Fluor Plus 555 anti-rat IgG antibody (A48263, Invitrogen), Alexa Fluor 488 anti-mouse IgG2b (A21141, Invitrogen), Alexa Fluor 488 anti-mouse IgG1 antibody (ab150117, Abcam), Alexa Fluor 647 anti-guinea pig IgG (A21450, Invitrogen), and Alexa Fluor 647 anti-rabbit IgG (A21245, Invitrogen).

## Mice

WT C57BL/6J (stock #000664), *Casp3* (*B6N.129S1-Casp3*$^{tm1Flv/J}$, stock #006233), *Gsdme* (*C57BL/6N-Gsdme*$^{em1Fsha/J}$, stock #032411), *Gsdmd* (*C57BL/6N-Gsdmd*$^{em4Fcw/J}$, stock #032410), and *Casp1/4* (*B6N.129S2-Casp1*$^{tm1Flv/J}$, stock #016621) KO mice were obtained from the Jackson Laboratory. *Ifnlr1*$^{f/f}$ mice were generated from *Ifnlr1*$^{tm1a(EUCOMM)Wtsi}$ ES cells and backcrossed to the C57BL/6J background as described previously (*7*). The *Ifnlr1*$^{f/f}$ mice were crossed to the *Deleter-Cre* line to generate the *Ifnlr1*$^{-/-}$ mice (*60*). *Gsdmd*$^{-/-}$*Gsdme*$^{-/-}$ DKO and littermate controls were generated by crossing aforementioned *Gsdmd*$^{-/-}$ and *Gsdme*$^{-/-}$ mouse lines. All mouse lines used in this study are C57BL/6J background.

WT and KO mice were bred and housed at the Brown University facilities under specific pathogen–free conditions with food and water ad libitum and 12-hour day-night cycle. The mice used were sex and age matched. Male and female mice were used at 8 to 12 weeks of age. All animal experiments were approved by Brown University Institutional Animal Care and Use Committee (protocol #23-04-0002). In experiments using *Casp3* mice, littermates from *Casp3*$^{+/-}$ × *Casp3*$^{+/-}$ breeding were used. For all other lines, KO × KO breeding was used with sex- and age-matched WT controls bred in the same facility.

For MNoV infection, adult mice at 8 to 12 weeks of age were inoculated with $10^6$ or $10^7$ plaque-forming units of CR6 or CW3 strain by the oral route in a volume of 25 μl or by intraperitoneal injection in a volume of 300-μl phosphate-buffered saline (PBS). Fecal pellets and tissues were harvested into 2-ml tubes (Sarstedt) with 1-mm-diameter zirconia/silica beads (Biospec). The samples were flash frozen by dry ice and stored at −80°C until analysis.

## Viruses

Stocks of MNoV strains CR6, CW3, and CR6$^{D121/131G}$ were generated from molecular clones. Briefly, plasmid encoding viral genomes of CR6 (MNoV GV/CR6/2005/USA, GenBank JQ237823) or CW3 (MNoV GV/MNV-1/2002/USA, clone CW3, GenBank EF014462.1) was transfected into human embryonic kidney (HEK) 293T cells to generate a P0 stock. Plasmid for CR6$^{D121/131G}$ was generated as previously described (*30*) and used for transfection. Supernatants were harvested at 48 hours post transfection, spun at 3000 rpm for 20 min, and passaged twice in BV2 cells. P2 virus supernatant was filtered and concentrated with Vivaflow 50 (Sartorius). Virus titer was determined via plaque assay. CR6 virus lacking the N-terminal region of NS3 (CR6ΔNS3) was generated as previously described (*10*).

## MNoV plaque assay

BV2 cells were plated in six-well plates and infected with serial dilutions of each viral stock or culture supernatants for 1 hour at room temperature. After removing the inoculum, the cells were overlaid with 1% methylcellulose (Sigma-Aldrich) in minimum essential medium (MEM, Gibco) supplemented with 5% fetal bovine serum (FBS), 1× penicillin-streptomycin, and 10 mM Hepes. The cells were incubated for 2 to 3 days and fixed and stained with 0.1% crystal violet/20% ethanol.

## Cell culture

BV2 (a gift of H. Virgin), iBMDM (mouse bone marrow-derived macrophages immortalized by stable expression of telomerase), IEC-M2C (derived from male mice) (*61*), Mx2LUC (purchased from Inscreenex, INS-CI-1007 L), and HEK293T (purchased from American Type Culture Collection, CRL-3216) cells were cultured in Dulbecco's modified Eagle's medium (Gibco) supplemented with 10% FBS and 2.5 mM Hepes (Gibco) at 37°C, 5% $CO_2$ and detached using 0.05% trypsin-EDTA (Gibco). For BV2 cells, blasticidin (5 μg/ml, Gibco), puromycin (2.5 μg/ml, Gibco), and G418 (400 μg/ml, Gibco) were added as appropriate. For IEC-M2C cells, blasticidin (5 μg/ml), hygromycin (200 μg/ml, Gibco), and puromycin (2 μg/ml) were added as appropriate. Expi293F cells (A14635, Thermo Fisher Scientific) were used to express the Fc proteins. The cells were maintained and expanded according to the Expi293 Expression System User Guide. They were grown in Expi293 medium at 37°C, 110 rpm, with 8% $CO_2$ atmosphere in plastic flasks with vented caps (Corning) in a $CO_2$ shaking incubator (Eppendorf).

## Generation of clonal KO lines

*Casp3* KO BV2 cell line (clone 2E10) generated in a previous study (*5*) was used. *Ninj1* KO BV2 cell lines (clone D7 and H4), *Gsdmd/e* DKO BV2 cell line (clone 1F3), and *Ninj1* KO iBMDM cell lines (clone 1A10 and 1G11) were generated at the Genome Engineering and iPSC center at Washington University School of Medicine, as previously described (*5*). sgRNA targeting each gene was nucleofected with Cas9 into WT cells. Clones were screened for frameshifts by sequencing the target region with Illumina MiSeq at approximately 500× coverage. sgRNA sequences and genomic sequences of the KO clones are provided in table S3.

## MNoV infection in vitro

For MNoV infection, BV2 cells were seeded at $1 \times 10^6$ cells per well of a six-well plate. After 16 hours, the cells were infected with MNoV

in 0.5-ml volume for 1 hour with gentle shaking at room temperature. Viral inoculum was removed, and 2 ml of the medium was added to the cells. For immunoblotting of secreted NS1 in the supernatant, the medium was replaced with VP-SFM with 1% Hepes at 4 hpi and harvested at indicated time points.

For NS1 ELISA and virion release assays, $2.5 \times 10^4$ cells were seeded in each well in 96-well plate. The following day, 20-μl volume of MNoV was added to cells for 5 multiplicity of infection (MOI) for BV2 and iBMDM cells or 20 MOI for IEC-M2C-CD300lf and IEC-Mx2LUC-CD300lf cells. The culture supernatant was harvested at 12 ~ 16 hpi for NS1 ELISA or at 16 hpi for virion titration by plaque assay as described above. When indicated, Q-VD-OPh (20 μM) and ganetespib/17-AAG/AT13885/quizartinib (2.4 nM ~ 10 μM) were added at the time of infection.

### Enteroid culture and infection

The mouse enteroid culture and infection were performed as previously described (*27*). Briefly, purified crypts from the mouse distal ileum were harvested and suspended in 30 μl of Matrigel (Corning, 356234) per well of a 24-well tissue plate. Six Hundred microliters of 50% L-WRN–conditioned medium (*62*, *63*) was added per Matrigel/enteroid [three-dimensional (3D) enteroid] well of a 24-well plate for culture. The medium was changed every 2 to 3 days, and the enteroids were split 1:8 every 7 days. For infection, the 3D enteroid were trypsinized to make single cells, and 100 μl of suspended cells were plated directly into the upper chamber Transwell inserts (Costar, 65-mm insert, 0.4-μm polyester membrane, 3470) and 600 μl of 50% L-WRN–conditioned medium with 10 mM Y27632 (Tocris, 1254) in the lower compartment was added. The next day, fresh mouse IntestiCult Organoid Growth Medium (STEMCELL Technologies, 06005) with recombinant IL-4 (50 ng/ml, Peprotech, 214-14) was added on the upper and lower compartments. The medium was replaced every 2 days and differentiated for ~14 days before being used for infections. For infections, the cells were apically infected with 100 μl of MNoV CR6 or CW3 at MOI of 0.5. After 1 hour, the unbound viruses were washed, and 150 μl of fresh mouse IntestiCult organoid growth medium was added on the apical compartment and 600 μl on the lower compartment. The apical supernatants were harvested at 48 hpi. The samples were frozen at −80°C until used for the NS1 ELISA.

### Plasmids

Gene fragments encoding WT CR6 NS1/2, triple-alanine scanning mutants, or point mutants were synthesized and inserted into pcDNA4/TO vector (Thermo Fisher Scientific) along with an N-terminal 2xStrep-tag II. Transient transfection of BV2 cells was performed using Lipofectamine LTX (Invitrogen) according to the manufacturer's instructions. For immunoblotting of secreted NS1 in the supernatant, the medium was replaced with VP-SFM with 1% Hepes at 6 hours post transfection and harvested after 24 hours.

For recombinant NS1 protein purification, WT CR6 NS1, truncation mutants, or triple-alanine mutants was subcloned into pET-15b (Novagen) with an N-terminal 6xHis tag. For recombinant NINJ1 protein purification, a codon-optimized open reading frame (ORF) of mouse NINJ1 ectodomain (residues 2 to 81), point mutants, or helix deletion mutants were inserted into pET-15b with an N-terminal maltose-binding protein (MBP) and 6xHis tag. For Fc-tagged NINJ1 protein purification, a codon-optimized ORF of human NINJ1 ectodomain (residues 2 to 81) was inserted to pcDNA3.1 (Thermo Fisher Scientific) with a C-terminal mouse IgG2b Fc tag.

### Lentivirus constructs and transduction

For lentivirus production, HEK293T cells were cotransfected with a desired lentivirus construct, packaging plasmids pMD2.G (Addgene, #12259) and psPAX2 (Addgene, #12260) using TransIT-LT1 (Mirus Bio). The medium was replaced with viral production medium 12 hours after transfection. The supernatant was collected, spun at 4347*g*, and filtered using a 0.45-μm filter (Millipore) at 36 hours after transfection.

BV2-Cas9 cells were generated by transducing pXPR101 (Broad Institute). IEC-M2C-CD300lf-Cas9 cells were generated by transducing pLX_311-Cas9 (Addgene, #96924) and pCDH-CMV-EF1-Hygro (System Biosciences) containing codon-optimized CD300lf (*64*). Individual sgRNAs targeting indicated genes (sequences provided in table S4) were cloned into linearized pLentiGuide-Puro (Addgene, #52963) for CRISPR KO.

BV2 cells were transduced by incubating 1 ml of harvested lentiviral stock and 1 ml of complete medium for 24 hours. IEC-M2C-CD300lf cells were transduced with 1 ml of harvested lentiviral stock, spun at 1200*g* for 90 min at 35°C with polybrene (1 μg/ml), and incubated for 18 hours after spin transduction. Two days after transduction, the cells were selected with appropriate drugs for 3 ~ 7 days.

To reconstitute NINJ1 or caspase-3 expression in clonal KO BV2 cells, a codon-optimized mouse NINJ1 ORF with an N-terminal 3xFLAG tag or mouse caspase-3 ORF was cloned into pCDH-MSCV-T2A-Puro (System Biosciences). K45Q and A59P point mutations were introduced by site-directed mutagenesis. For inducible Tet-on system, 2xStrep-tagged WT or mutated NS1/2 coding sequences were cloned into pLVX-TRE3G vector (Clontech). BV2 cells grown in tetracycline-free medium were cotransduced with lentiviruses generated with pLVX-EF1a-Tet3G (Clontech) and pLVX-TRE3G-NS1/2 WT or mutant constructs. The cells were selected with G418 and puromycin, and gene expression was induced with doxycycline (2 μg/ml).

### Quantitative reverse transcription PCR

RNA was isolated from stool using Quick-RNA Viral 96 kits (R1041, Zymo). RNA from tissues or cells were isolated using TRI reagent with Direct-zol-96 RNA kits (R2057, Zymo) according to the manufacturer's protocol. Five microliters of RNA from stool or 1 μg of RNA from tissue was used for cDNA synthesis with the ImPromII reverse transcriptase system (PAA3803, Promega). MNoV TaqMan assays were performed, using a standard curve for determination of absolute viral genome copies. Quantitative polymerase chain reaction (PCR) for housekeeping gene *Rps29* was performed with forward primer 5′-GCAAATACGGGCTGAACATG-3′, reverse primer 5′-GTCCAACTTAATGAAGCCTATGTC-3′, and probe 5′ /5HEX/CCTTCGCGT/ZEN/ACTGCCGGAAGC/3IABkFQ/-3′ (synthesized at IDT), each at a concentration of 0.2 μM, using AmpliTaq Gold DNA polymerase (4311818, Applied Biosystems). Predesigned PrimeTime qPCR assays (IDT) were used to quantify expression of mouse *Gsdmd* (Mm.PT.58.30932133) and *Gsdme* (Mm.PT.58.5215813). Standard curves for quantitative PCR assays were used to facilitate absolute quantification of transcript copy numbers.

### Flow cytometry

To measure the expression of viral proteins, the cells were fixed with Cytofix/Cytoperm buffer (BD Bioscience) for 10 min at room

temperature, followed by washing twice with Perm/Wash buffer (BD Biosciences). Cells were stained with anti-NS1 (CM79 or 2A9; 1:200), anti-NS6/7 (1:2,000), and anti-VP1 (1:200) for 1 hour at 4°C. Cells were subsequently stained with FITC anti-mouse IgG2b (BioLegend), PE anti-guinea pig (Jackson ImmunoResearch), and Alexa Fluor 647 anti-mouse IgG2a (BioLegend) for 30 min. After washing, the cells were analyzed using FACSCelesta (BD Biosciences) or Cytek Aurora spectral analyzer (Cytek Biosciences). Data were analyzed with Flowjo software. To measure caspase-3 activation, the cells were stained with an antibody for cleaved caspase-3 (clone C92-605, BD Biosciences) and PE anti-rabbit IgG (Jackson ImmunoResearch). To measure cell death, the cells were first stained with LIVE/DEAD Fixable Aqua stain (Thermo Fisher Scientific) for 30 min on ice, washed, and stained with PE/cyanine7 annexin V (BioLegend) for 15 min at room temperature, followed by fixation/permeabilization as described above for intracellular staining.

### Genome-wide CRISPR KO screen

A mouse genome-wide CRISPR KO Brie library containing four sgRNAs per gene was used (*31*). BV2-Cas9 cells ($2.16 \times 10^8$) were transduced with the library at ~0.3 MOI to make $6.4 \times 10^7$ transduced cells, which is sufficient for the integration of each sgRNA into ~800 cells. The following day, puromycin was added and cells were selected for 5 days.

For the screen, a total of $2.4 \times 10^8$ cells were seeded in 15-cm dishes at a density of $6 \times 10^5$ cells/ml and infected with CR6 virus at 5 MOI the following day. Infected cells were harvested at 16 hpi. The suspended cells were harvested as well to include dying cells. Cells were fixed and stained as described above using anti-NS1 (CM79) and anti-NS6/7. FITC-conjugated anti-mouse IgG1 and Alexa Fluor 647–conjugated anti-guinea pig IgG were used as secondary antibodies, and after staining, the cells were subjected to sorting using FACSAriaIII (BD Biosciences). $NS1^-NS6/7^+$ (~60% of total cells) and $NS1^+NS6/7^+$ (~20% of total cells) were isolated separately. After sorting, $1.04 \times 10^7$ and $2.88 \times 10^7$ were obtained. Genomic DNA (gDNA) was extracted from the isolated cells with QIAamp DNA Maxi kit (Qiagen).

### CRISPR screen sequencing and analysis

Illumina sequencing and analysis were performed as previously described (*41*). Briefly, gDNA samples were PCR amplified using Titanium Taq DNA polymerase (639209, Takara), P5 stagger primer mix (0.5 μM) and uniquely barcoded P7 primer (0.5 μM). PCR products were pooled and purified with AMPure XP beads (MSPP-A63880, Beckman Coulter). Samples were sequenced on a NextSeq550 sequencer (Illumina). Reads were demultiplexed with barcodes and then mapped to a reference file of sgRNAs using LibraryAligner (https://gitlab.com/buchserlab/library-aligner). We calculated the log-fold change of sgRNAs between NS1-negative cells and NS1-positive cells and calculated the hypergeometric distribution to determine *P* values.

### NS1 ELISA

Ninety-six–well EIA/RIA flat bottom plates (Corning) were coated with anti-NS1 (2 μg/ml, clone 11G10, recognizing the epitope 1 to 31 amino acids) using BD OptEIA Reagent Set B (BD) at 4°C, overnight. After blocking with 2% FBS in PBS, the plates were incubated with diluted supernatant samples or recombinant NS1 protein standards for 4 hours at 4°C. The plates were incubated with 0.25 μg of the second anti-NS1 (clone 2A9, recognizing the epitope 32 to 48 amino acids), followed by the incubation of HRP anti-mouse IgG2b (Southern Biotech) at 1:2000 dilution. Trimethylboron (TMB) substrate (Thermo Fisher Scientific) was added to the plates and quenched with stop solution (Thermo Fisher Scientific). Absorbance at 450 nm was measured using BioTek synergy HT microplate reader.

This NS1 ELISA assay does not differentiate between NS1, NS1/2, or the precursor polypeptide NS1/2/3/4/5/6/7. This ELISA assay was performed on culture supernatant, where NS1 is the predominant form detected, with uncleaved NS1/2 constituting less than 5% at the tested time points. This predominance was confirmed through paired immunoblot assays when the NS1 ELISA was used.

### Cell death assay

BV2, iBMDM, or IEC-M2C-CD300lf cells ($2.5 \times 10^4$) were seeded in each well in 96-well plate. The following day, 20-μl volume of MNoV was added to cells for 5 MOI. For apoptotic stimulation, 40 μM etoposide or 1 μM staurosporine was added. For pyroptotic stimulation, the cells were primed with LPS (100 ng/ml) for 12 hours, followed by stimulation with 3 mM ATP or 20 μM nigericin. After infection or stimulation, 250 nM Sytox Orange (Thermo Fisher Scientific) was added. Fluorescence was measured using BioTek synergy HT microplate reader at indicated time points. Culture supernatants were analyzed for LDH release using CyQUANT LDH cytotoxicity assay kit (Thermo Fisher Scientific). The cells treated with 0.2% Tween-20 were used as a positive control for cell death. When indicated, 5 mM glycine was added after MNoV infection.

### Immunoblot and immunoprecipitation

Cells were lysed in radioimmunoprecipitation assay lysis and extraction buffer (Thermo Fisher Scientific) with Complete Protease Inhibitor (Roche) for 10 min at 4°C and spun down at 18,000*g* for 30 min. Protein concentration of the cell lysate was measured by Pierce bicinchoninic acid (BCA) assay (Thermo Fisher Scientific). Lysate was mixed with Laemmli sample buffer (Bio-Rad) supplemented with 2-mercaptoethanol (Sigma-Aldrich) and boiled for 10 min. To detect secreted proteins, the culture supernatant was spun down and filtered with a 0.2-μm syringe filter to remove cellular debris. The filtered supernatant was precipitated with TCA (Sigma-Aldrich) at final 20% concentration by volume on ice for 10 min. TCA-precipitated supernatant was centrifuged at 18,000*g* for 15 min at 4°C and washed with ice-cold acetone. The protein pellets were resuspended in 1× SDS-reducing sample buffer and boiled for 5 min. Protein samples were separated by SDS-PAGE using 4 to 20% Mini-PROTEAN TGX Stain-Free Protein Gels (Bio-Rad), transferred to 0.45-μm polyvinylidene difluoride (PVDF) membrane (Bio-Rad), blocked with Intercept [tris-buffered saline (TBS)] blocking buffer (Li-Cor), and probed with indicated antibodies. Signals were visualized with ChemiDoc MP Imaging System (Bio-Rad). Band intensity was quantified using ImageJ software.

For anti-NS1 immunoprecipitation, BV2 cells were infected with CR6 at 5 MOI and harvested at 10 hpi. Cells were washed twice with cold PBS and lysed with 50 mM tris-HCl (pH 7.5), 150 mM NaCl, 1 mM EDTA, 2 mM MgCl2, 1% Triton X-100, and the Complete Protease Inhibitor (Sigma-Aldrich). The lysates were incubated on ice for 30 min and before being spun down for 30 min at 18,000*g* at 4°C. Protein concentration was measured by BCA assay. A 2-mg volume of total protein was mixed with 10 μg of anti-NS1 monoclonal antibody (2A9) or mouse IgG2b isotype control (BioXCell), which was preincubated with Dynabeads Protein G (Thermo Fisher Scientific) for 1 hour at 4°C. The mixture was incubated overnight at 4°C

with rotation and washed three times with lysis buffer. Proteins were eluted by 2× SDS sample buffer and boiled for 5 min before running on SDS-PAGE.

### Native PAGE

BV2 cells infected with CR6 at 5 MOI were harvested at 10 hpi and lysed for 10 min at 4°C in 50 mM tris-HCl (pH 7.5), 150 mM NaCl, supplemented with 1% digitonin (Thermo Fisher Scientific) and the Complete Protease Inhibitor (Sigma-Aldrich). Cells were scraped, incubated for additional 10 min at 4°C with rotation, and spun down at 20,000*g* for 15 min. Protein concentration was measured by BCA assay, and normalized lysate was mixed with Native sample buffer (Bio-Rad). Samples were run on 4 to 20% Mini-PROTEAN TGX Stain-Free Protein Gels (Bio-Rad) with tris/glycine buffer without SDS, transferred to PVDF membranes, and immunoblotted as described above.

### Secretome analysis

BV2 cells ($5 \times 10^5$) were seeded per well in 24-well plates. The following day, the cells were infected with MNoV in 0.5-ml volume at 5 MOI for 1 hour with gentle rocking at room temperature. Viral inoculum was removed, and 2 ml of the medium was added to the cells. After 2 hours, the cells were washed and replaced with VP-SFM to remove serum proteins and harvested at 16 hpi. The supernatant was concentrated with TCA as described above along with human IgG1 included in each sample as a spike-in and subjected to SDS-PAGE. Samples were run using 4 to 20% Mini-PROTEAN TGX Precast Protein Gels (Bio-Rad) for 1 cm, and the gels were fixed, stained with Coomassie blue R-250, sliced, and submitted to University of Texas Southwestern Proteomics Core for liquid chromatography tandem MS (LC-MS/MS) analysis.

Samples were digested overnight with trypsin (Pierce) following reduction and alkylation with dithiothreitol (DTT) and iodoacetamide (Sigma-Aldrich). The samples then underwent solid-phase extraction cleanup with an Oasis HLB plate (Waters), and the resulting samples were injected onto a Q Exactive HF mass spectrometer coupled to an Ultimate 3000 RSLC-Nano LC system. Samples were injected onto a 75 μm i.d., 15-cm-long EasySpray column (Thermo Fisher Scientific) and eluted with a gradient from 0 to 28% buffer B over 90 min. Buffer A contained 2% (v/v) acetonitrile (ACN) and 0.1% formic acid in water, and buffer B contained 80% (v/v) ACN, 10% (v/v) trifluoroethanol, and 0.1% formic acid in water. The mass spectrometer operated in positive ion mode with a source voltage of 2.6 kV and an ion transfer tube temperature of 300°C. MS scans were acquired at 120,000 resolution in the Orbitrap, and up to 20 MS/MS spectra were obtained in the ion trap for each full spectrum acquired using higher-energy collisional dissociation for ions with charges 2 to 8. Dynamic exclusion was set for 20 s after an ion was selected for fragmentation.

Raw MS data files were analyzed using Proteome Discoverer v3.0 SP1 (Thermo Fisher Scientific), with peptide identification performed using a tryptic search with Sequest HT against the mouse reviewed protein database from UniProt (17,062 sequences) along with the human IgG1 protein from UniProt and MNoV strain CR6 proteins. Fragment and precursor tolerances of 10 ppm and 0.02 Da were specified, and three missed cleavages were allowed. Carbamidomethylation of Cys was set as a fixed modification, with oxidation of Met set as a variable modification. The false discovery rate cutoff was 1% for all peptides. Protein abundance was normalized to human IgG1 spike-in protein and then analyzed using Perseus software v.2.0.11 (*65*). Data were $\log_2$ transformed, missing values were imputed by normal distribution with a width of 0.3 and down shift of 1.8, and differential protein abundances between groups were tested with a two-tailed Student's *t* test.

### ELISA to measure antibody responses

Immulon-2HB ELISA plates were coated with recombinant NS1, NS2, NS6/7, or CR6 viral stock, followed by blocking with assay diluent in BD OptEIA Reagent Set B (BD). Serum samples were heat-inactivated for 30 min at 56°C and diluted 100-, 1000-, and 10,000-fold in the assay diluent. Diluted serum was incubated in the coated plate for 2 hours at room temperature. For standard curve, serial dilutions of isotype mouse IgG were coated. For positive quantification controls, mouse monoclonal anti-NS1 (CM79) and anti-VP1 (A6.2), rabbit polyclonal anti-NS2 (R696, this study), and guinea pig polyclonal anti-NS6/7 (GP97, this study) were used. Anti-NS2 (R696) and anti-NS6/7 (GP97) were generated by immunizing animals with the same recombinant proteins used in the ELISA. HRP-conjugated secondary antibodies detecting mouse, rabbit, or guinea pig IgG (Southern Biotech) were used at a dilution of 1:5000. TMB substrates were added, and plates were analyzed as described above.

### Protein structure visualization

A 3D structure of MNoV CR6 NS1 (G58-R114) has been previously determined using solution NMR (PDB: 2MCK) (*39*) and was visualized using ChimeraX software (*66*).

### Immunofluorescent staining and image analysis

BV2 cells ($2 \times 10^4$) were seeded per well in eight-well chamber slides (Nunc). The following day, 20-μl volume of MNoV was added to cells for 5 MOI and harvested at 10 hpi. BV2 cells were fixed with 4% formaldehyde in PBS for 20 min, 0.1% Triton X-100 for 10 min in PBS, and blocked with 10% goat serum for 1 hour. To detect NINJ1 protein, viral antigens, different organelles and anti-DYKDDDDK tag antibody (BioLegend, 1:100), in-house monoclonal anti-NS1 (clone 2A9 and clone CM79, 1:1000) and anti-NS6/7 (1:1000), calnexin (ER marker, Abcam, 1:1000), Rab7 (endosome marker, Abcam, 1:1000), ATP5A1 (mitochondrial marker, Thermo Fisher Scientific, 1:1000), and TGN46 (Golgi marker, Abcam, 1:1000) antibodies were used, followed by second antibodies incubation. The cells were incubated with Alexa Fluor Plus 555–conjugated goat anti-rat IgG antibody (Invitrogen), Alexa Fluor 647–conjugated goat anti-rabbit IgG antibody (Invitrogen), Alexa Fluor 647–conjugated goat anti-guinea pig IgG antibody (Invitrogen), Alexa Fluor 488–conjugated goat anti-mouse IgG2b antibody (Invitrogen), Alexa Fluor 647–conjugated rat anti-mouse IgG2a antibody (BioLegend), and Phalloidin-iFluor 647 (Abcam) for 1 hour. The coverslips were mounted on a slide using Prolong glass antifade mountant with NucBlue (Invitrogen). The fluorescence images were recorded using a Zeiss microscope. Colocalization analysis was performed by calculating the Pearson's correlation coefficient with the JACoP as implemented in ImageJ (*67*). In addition, the number and proportion of NINJ1 speckles that overlaps with NINJ1 through colocalization and distance analysis using the DiAna method that quantifies protein-protein colocalization in 3D-reconstituted images (*68*). For Sytox Green staining, BV2 cells were seeded as described above and infected with MNoV at 5 MOI or treated with etoposide (40 μM). A total of 250 nM Sytox Green (Thermo Fisher Scientific) was added

and cells harvested after 16 hours, fixed with 4% formaldehyde in PBS, and analyzed with fluorescent microscopy.

### Transmission electron microscopy

For immunolocalization at the ultrastructural level, the cells were fixed in 4% paraformaldehyde (Electron Microscopy Sciences) in 100 mM PIPES (Electron Microscopy Sciences), pH 7.2 for 1 hour at 4°C. Samples were then embedded in 10% gelatin and infiltrated overnight with 2.3 M sucrose/20% polyvinyl pyrrolidone in PIPES at 4°C. The samples were trimmed, frozen in liquid nitrogen, and sectioned with a Leica Ultracut UCT7 cryo-ultramicrotome (Leica Microsystems). Ultrathin sections of 50 nm were blocked with 5% FBS/5% normal goat serum for 30 min and subsequently incubated with rat anti-FLAG and mouse anti-NS1 antibodies for 1 hour at room temperature. Following washes in block buffer, sections were subsequently incubated with goat anti-rat IgG (H + L) conjugated to 12-nm colloidal gold and goat anti-mouse conjugated to 18-nm colloidal gold (Jackson ImmunoResearch Laboratories) for 1 hour. Sections were stained with 0.3% uranyl acetate/2% methyl cellulose and viewed on a JEOL 1200 EX transmission electron microscope (JEOL USA) equipped with an AMT 8-megapixel digital camera and AMT Image Capture Engine V602 software (Advanced Microscopy Techniques). All labeling experiments were conducted in parallel with controls omitting the primary antibodies, both or individually, to confirm that there was no nonspecific binding or cross-reactivity of the secondary antibodies.

### Recombinant protein purification

The constructs for recombinant protein expression were introduced into *E. coli* BL21 (DE3). Proteins were induced at an optical density at 600 nm of 0.6 with isopropyl β-D-1-thiogalactopyranoside and incubated for 18 to 20 hours at 16°C. Cells were pelleted by centrifugation at 4000*g* and resuspended in lysis buffer composed of TBS (pH 7.4), 10 mM $MgCl_2$, 10 mM $CaCl_2$, 20 mM DTT, 0.5% Triton X-100, supplemented with lysozyme, deoxyribonuclease I, and 4-benzenesulfonyl fluoride hydrochloride. Cells were lysed using a Digital Sonifier (Branson) using 3 s–by–30 s bursts and centrifuged at 20,000*g* for 20 min to remove cell debris and precipitation. The resultant supernatant was purified using a nickel nitrilotriacetic acid column before buffer exchange to TBS and concentration. Final protein samples were subject to purity-check by SDS-PAGE followed by Coomassie blue staining, and protein concentration was measured by Pierce BCA assay (Thermo Fisher Scientific).

For Fc-tagged protein purification, plasmids encoding ectodomains of human or mouse NINJ1 were transfected into $7.5 \times 10^6$ Expi293F cells in 25 ml of Expression medium using the Expi-Fectamine293 transfection kit (Thermo Fisher Scientific) and Opti-MEM (Gibco). Enhancers 1 and 2 were added 18 to 22 hours posttransfection, as per the Expi293 User Guide. The cultures were expanded for 5 days for protein expression. Cell viability and count were routinely monitored using a trypan blue exclusion assay. The cell pellet was separated from the supernatant by centrifugation. The supernatant was filtered using a 0.45-μm membrane to remove cell debris and precipitation. Protein G (Thermo Fisher Scientific) was added to the purified supernatant, and the mixture was rocked at 4°C overnight. The solution was loaded onto Econo-Pac chromatography columns, which were then washed three times with PBS. The protein was eluted with 0.2 M glycine (pH 2.0), and an equal volume of 2 M tris base (pH 9.0) was added to the eluate. Last, the eluate was buffer-exchanged with PBS. Final protein samples were checked for purity by SDS-PAGE, and concentration was measured.

### ELISA binding assay

To investigate the binding of NS1-His and Fc-NINJ1 protein purified in house, ELISA assays were performed on immobilized NS1 protein. Ninety-six–well EIA/RIA plates (Corning) were coated with NS1 protein (2 μg/ml) at 4°C overnight, followed by 1 hour of blocking buffer containing 1× Hanks' balanced salt solution (HBSS, Gibco) and 2% FBS. The plates were then incubated with serially diluted monoclonal NS1 antibody (CM79), Fc-tagged human NINJ1 protein, or mouse IgG2b isotype control for 2 hours. The plate was then incubated with HRP-conjugated anti-mouse IgG (Southern Biotech) for 1 hour at room temperature. Next, TMB substrate (Thermo Fisher Scientific) were added to the plates and then quenched with stop solution (Thermo Fisher Scientific). Absorbance at 450 nm was recorded with a BioTek synergy HT microplate reader. Three washes were performed between every incubation using 1× HBSS with 0.05% Tween-20. GraphPad Prism software was set to perform nonlinear regression curve-fitting analyses of binding data to estimate dissociation constant ($K_d$).

A different set of ELISA assays were performed using recombinant human NINJ1-His protein (9717-NJ-050, R&D) or mouse NINJ1-His protein purified in-house. ELISA was performed as described above, with plate coated with NINJ1 proteins first and then incubated with serially diluted NS1-His or bovine serum albumin (BSA) control protein. The plate was incubated with in-house monoclonal anti-NS1 (5 μg/ml, clone 11G10) and then with HRP-conjugated rabbit anti-hamster IgG (Southern Biotech) for 1 hour at room temperature and analyzed as described above.

To determine the epitope of monoclonal anti-NS1 antibodies, ELISA assays were performed using a series of truncation mutant NS1 proteins purified in house. Ninety-six–well plates were coated with MBP-His-NS1 (2 μg/ml) full-length ("1 to 121") or mutants with 1 to 31, 1 to 47, and 1 to 64 residues deleted (labeled as "32–121", "48–121," and "65–121"). After overnight coating at 4°C and blocking, the plates were incubated with serially diluted anti-NS1 antibodies, CM79 and 2A9 (starting concentration, 10 μg/ml). Following 1-hour incubation at room temperature, the plates were incubated with HRP-conjugated anti-mouse IgG1 (Southern Biotech) for CM79 and anti-mouse IgG2b (Southern Biotech) for 2A9 and then analyzed as described above.

### Microscale thermophoresis

MST analysis was performed using a NanoTemper Monolith X instrument (NanoTemper Technologies). Target proteins were set to purified recombinant murine NINJ1 (MBP-His-mNINJ1) proteins, including WT and K45Q or A59P-substituted mutants and Helix 1 (Δα1) or Helix 2 (Δα2)–truncated mutants. The target proteins were incubated with the RED-NHS 2nd Generation dye (#MO-L011, Nanotemper Technologies) for 30 min and separated from free dye. Then, these fluorescently labeled target proteins were diluted to final 25 nM in assay buffer [25 mM tris-HCl (pH 7.5), 13 mM NaCl, 2.7 mM KCl, and 0.05% Triton X-100) to be mixed with the serial diluted ligands including the purified recombinant 6xHis-tagged CR6 NS1 proteins and 6xHis-tagged MBP-His as a negative control. The NS1 proteins were serially diluted in assay buffer for a 1:2 dilution series with a final concentration of 200 μM down to 6.1 nM for WT murine NS1, 90 μM down to 2.75 nM for Ala-mutated murine NS1

proteins, 68.5 μM down to 2.01 nM for truncated murine NS1 proteins, and 70 μM down to 2.14 nM for MBP-His protein. Labeled target proteins were added in a 1:1 ratio to ligand proteins followed by preincubating for 30 min at room temperature and loaded into standard capillaries (#MO-K022, Nanotemper Technologies). Capillaries were then subjected to Monolith X for MST analysis. According to Monolith guidelines, signal-to-noise ratios greater than 5.0 were indicated as the valid binding. $K_d$s were calculated using normalized fluorescence (Fnorm = F1/F0; F0: initial 670-nm fluorescence, F1: 670 nm fluorescence at 5 s after heating) via the NanoTemper software from independent triplicate MST experiments. The dose-response curves of each MST assays were plotted using the change in the normalized fluorescence (ΔFnorm).

### Lipid overlay assay

Lipid overlay assays were performed using lipid strips purchased from Echelon Biosciences. Lipid strips were blocked in assay buffer, 3% BSA in TBS with 0.1% Tween-20 (TBS-T), for 1 hour and incubated with purified WT or mutant NS1 proteins (1 μg/ml) at 4°C overnight. The strips were washed three times with TBS-T and immunoblotted with anti-His antibody.

### Isothermal titration calorimetry

ITC was performed using purified His-NS1 protein and water-soluble analogs of PI(3)P and PI(5)P, PI(3)P-diC8, and PI(5)P-diC8, purchased from Echelon Biosciences. ITC was performed by Creative Biolabs. The titrations were performed at 20°C in buffer containing 50 mM tris (pH 7.5) and 150 mM NaCl with a speed of 250 rpm using Nano ITC (TA Instruments). Two-microliter aliquots of PI(3)P-diC8 (200 μM) and PI(5)P-diC8 (300 μM) were injected from a syringe into the sample cell containing 350 μl of His-NS1 (20 μM). Each experiment was accompanied by the corresponding control experiment in which 2.5-μl aliquots of PIPs were injected into a solution of buffer alone to measure the dilution heat, which was subtracted from the protein data. The delay between injections was 150 s. Each injection generated a heat burst curve, and data were analyzed by Origin software.

### Drug screen

DiscoveryProbe FDA-approved Drug Library was purchased from ApexBio (L1021), which includes 2320 FDA-approved drugs prepared in 10 mM. BV2 cells ($2.5 \times 10^4$) were seeded per well in 96-well plates. The following day, 20-μl volume of MNoV was added to cells for 5 MOI along with 250 nM Sytox Orange (Thermo Fisher Scientific) and drugs diluted for final 10 μM. At 16 hpi, cell death was monitored by measuring Sytox uptake, and the supernatant was harvested and subjected to NS1 ELISA as described above. %NS1 secretion was calculated relative to vehicle-treated wells. The screen was performed in two biological replicates, and drugs showing >50% reduced NS1 secretion were selected for further analysis. To determine the $IC_{50}$ values, fourfold serial dilutions were made for each drug and analyzed with four biological replicates.

### Drug administration in mice

Ganetespib (50 mg/kg, Apexbio) formulated in DRD (10% dimethyl sulfoxide, 18% Cremorphor RH 40 and 3.6% dextrose to prevent precipitation) was used. Mice were intravenously injected with placebo or ganetespib 1 day before infection, and day 1 and day 3 post-infection. Mice stool and tissue samples were harvested at day 3 and day 7.

### Statistical analysis

Statistical significance was determined using GraphPad Prism 10 software. Experiments were analyzed by one-way analysis of variance (ANOVA) with Kruskal-Wallis test, Dunnett's multiple comparisons test, or Tukey's multiple comparisons test and two-tailed unpaired Mann-Whitney test as indicated.

## Supplementary Materials

**The PDF file includes:**

Figs. S1 to S8
Legends for tables S1 and S2
Tables S3 and S4

**Other Supplementary Material for this manuscript includes the following:**

Tables S1 and S2

## REFERENCES AND NOTES


1. N. Kayagaki, O. S. Kornfeld, B. L. Lee, I. B. Stowe, K. O'Rourke, Q. Li, W. Sandoval, D. Yan, J. Kang, M. Xu, J. Zhang, W. P. Lee, B. S. McKenzie, G. Ulas, J. Payandeh, M. Roose-Girma, Z. Modrusan, R. Reja, M. Sagolla, J. D. Webster, V. Cho, T. D. Andrews, L. X. Morris, L. A. Miosge, C. C. Goodnow, E. M. Bertram, V. M. Dixit, NINJ1 mediates plasma membrane rupture during lytic cell death. *Nature* **591**, 131–136 (2021).
2. N. Kayagaki, I. B. Stowe, K. Alegre, I. Deshpande, S. Wu, Z. Lin, O. S. Kornfeld, B. L. Lee, J. Zhang, J. Liu, E. Suto, W. P. Lee, K. Schneider, W. Lin, D. Seshasayee, T. Bhangale, C. Chalouni, M. C. Johnson, P. Joshi, J. Mossemann, S. Zhao, D. Ali, N. M. Goldenberg, B. A. Sayed, B. E. Steinberg, K. Newton, J. D. Webster, R. L. Kelly, V. M. Dixit, Inhibiting membrane rupture with NINJ1 antibodies limits tissue injury. *Nature* **618**, 1072–1077 (2023).
3. M. Degen, J. C. Santos, K. Pluhackova, G. Cebrero, S. Ramos, G. Jankevicius, E. Hartenian, U. Guillerm, S. A. Mari, B. Kohl, D. J. Muller, P. Schanda, T. Maier, C. Perez, C. Sieben, P. Broz, S. Hiller, Structural basis of NINJ1-mediated plasma membrane rupture in cell death. *Nature* **618**, 1065–1071 (2023).
4. L. David, J. P. Borges, L. R. Hollingsworth, A. Volchuk, I. Jansen, E. Garlick, B. E. Steinberg, H. Wu, NINJ1 mediates plasma membrane rupture by cutting and releasing membrane disks. *Cell* **187**, 2224–2235.e16 (2024).
5. S. Lee, H. Liu, C. B. Wilen, Z. E. Sychev, C. Desai, B. L. Hykes Jr., R. C. Orchard, B. T. McCune, K. W. Kim, T. J. Nice, S. A. Handley, M. T. Baldridge, G. K. Amarasinghe, H. W. Virgin, A secreted viral nonstructural protein determines intestinal norovirus pathogenesis. *Cell Host Microbe* **25**, 845–857.e5 (2019).
6. S. Lee, C. B. Wilen, A. Orvedahl, B. T. McCune, K. W. Kim, R. C. Orchard, S. T. Peterson, T. J. Nice, M. T. Baldridge, H. W. Virgin, Norovirus cell tropism is determined by combinatorial action of a viral non-structural protein and host cytokine. *Cell Host Microbe* **22**, 449–459.e4 (2017).
7. T. J. Nice, M. T. Baldridge, B. T. McCune, J. M. Norman, H. M. Lazear, M. Artyomov, M. S. Diamond, H. W. Virgin, Interferon-λ cures persistent murine norovirus infection in the absence of adaptive immunity. *Science* **347**, 269–273 (2015).
8. J. L. Hyde, J. M. Mackenzie, Subcellular localization of the MNV-1 ORF1 proteins and their potential roles in the formation of the MNV-1 replication complex. *Virology* **406**, 138–148 (2010).
9. K. Ettayebi, M. E. Hardy, Norwalk virus nonstructural protein p48 forms a complex with the SNARE regulator VAP-A and prevents cell surface expression of vesicular stomatitis virus G protein. *J. Virol.* **77**, 11790–11797 (2003).
10. G. Wang, D. Zhang, R. C. Orchard, D. C. Hancks, T. A. Reese, Norovirus MLKL-like protein initiates cell death to induce viral egress. *Nature* **616**, 152–158 (2023).
11. C. E. Wobus, The dual tropism of noroviruses. *J. Virol.* **92**, e01010-17 (2018).
12. S. Lee, Norovirus cell tropism: The road to uncovering its secret hideout. *Cell Host Microbe* **30**, 454–457 (2022).
13. C. B. Wilen, S. Lee, L. L. Hsieh, R. C. Orchard, C. Desai, B. L. Hykes Jr., M. R. McAllaster, D. R. Balce, T. Feehley, J. R. Brestoff, C. A. Hickey, C. C. Yokoyama, Y. T. Wang, D. A. MacDuff, D. Kreamalmayer, M. R. Howitt, J. A. Neil, K. Cadwell, P. M. Allen, S. A. Handley, M. van Lookeren Campagne, M. T. Baldridge, H. W. Virgin, Tropism for tuft cells determines immune promotion of norovirus pathogenesis. *Science* **360**, 204–208 (2018).
14. V. R. Graziano, M. M. Alfajaro, C. O. Schmitz, R. B. Filler, M. S. Strine, J. Wei, L. L. Hsieh, M. T. Baldridge, T. J. Nice, S. Lee, R. C. Orchard, C. B. Wilen, CD300lf conditional knockout mouse reveals strain-specific cellular tropism of murine norovirus. *J. Virol.* **95**, e01652-20 (2021).

15. C. E. Wobus, S. M. Karst, L. B. Thackray, K. O. Chang, S. V. Sosnovtsev, G. Belliot, A. Krug, J. M. Mackenzie, K. Y. Green, H. W. Virgin, Replication of norovirus in cell culture reveals a tropism for dendritic cells and macrophages. *PLoS Biol.* **2**, e432 (2004).
16. M. K. Jones, M. Watanabe, S. Zhu, C. L. Graves, L. R. Keyes, K. R. Grau, M. B. Gonzalez-Hernandez, N. M. Iovine, C. E. Wobus, J. Vinje, S. A. Tibbetts, S. M. Wallet, S. M. Karst, Enteric bacteria promote human and mouse norovirus infection of B cells. *Science* **346**, 755–759 (2014).
17. S. M. Karst, C. E. Wobus, I. G. Goodfellow, K. Y. Green, H. W. Virgin, Advances in norovirus biology. *Cell Host Microbe* **15**, 668–680 (2014).
18. D. W. Strong, L. B. Thackray, T. J. Smith, H. W. Virgin, Protruding domain of capsid protein is necessary and sufficient to determine murine norovirus replication and pathogenesis in vivo. *J. Virol.* **86**, 2950–2958 (2012).
19. T. J. Nice, D. W. Strong, B. T. McCune, C. S. Pohl, H. W. Virgin, A single-amino-acid change in murine norovirus NS1/2 is sufficient for colonic tropism and persistence. *J. Virol.* **87**, 327–334 (2013).
20. T. J. Nice, L. C. Osborne, V. T. Tomov, D. Artis, E. J. Wherry, H. W. Virgin, Type I interferon receptor deficiency in dendritic cells facilitates systemic murine norovirus persistence despite enhanced adaptive immunity. *PLOS Pathog.* **12**, e1005684 (2016).
21. V. T. Tomov, O. Palko, C. W. Lau, A. Pattekar, Y. Sun, R. Tacheva, B. Bengsch, S. Manne, G. L. Cosma, L. C. Eisenlohr, T. J. Nice, H. W. Virgin, E. J. Wherry, Differentiation and protective capacity of virus-specific $CD8^+$ T cells suggest murine norovirus persistence in an immune-privileged enteric niche. *Immunity* **47**, 723–738.e5 (2017).
22. V. T. Tomov, L. C. Osborne, D. V. Dolfi, G. F. Sonnenberg, L. A. Monticelli, K. Mansfield, H. W. Virgin, D. Artis, E. J. Wherry, Persistent enteric murine norovirus infection is associated with functionally suboptimal virus-specific CD8 T cell responses. *J. Virol.* **87**, 7015–7031 (2013).
23. M. S. Strine, E. Fagerberg, P. W. Darcy, G. M. Barron, R. B. Filler, M. M. Alfajaro, N. D'Angelo-Gavrish, F. Wang, V. R. Graziano, B. L. Menasche, M. Damo, Y. T. Wang, M. R. Howitt, S. Lee, N. S. Joshi, D. Mucida, C. B. Wilen, Intestinal tuft cell immune privilege enables norovirus persistence. *Sci. Immunol.* **9**, eadi7038 (2024).
24. K. A. Chachu, D. W. Strong, A. D. LoBue, C. E. Wobus, R. S. Baric, H. W. Virgin IV, Antibody is critical for the clearance of murine norovirus infection. *J. Virol.* **82**, 6610–6617 (2008).
25. K. A. Chachu, A. D. LoBue, D. W. Strong, R. S. Baric, H. W. Virgin, Immune mechanisms responsible for vaccination against and clearance of mucosal and lymphatic norovirus infection. *PLOS Pathog.* **4**, e1000236 (2008).
26. K. R. Grau, S. Zhu, S. T. Peterson, E. W. Helm, D. Philip, M. Phillips, A. Hernandez, H. Turula, P. Frasse, V. R. Graziano, C. B. Wilen, C. E. Wobus, M. T. Baldridge, S. M. Karst, The intestinal regionalization of acute norovirus infection is regulated by the microbiota via bile acid-mediated priming of type III interferon. *Nat. Microbiol.* **5**, 84–92 (2020).
27. M. S. Strine, M. M. Alfajaro, V. R. Graziano, J. Song, L. L. Hsieh, R. Hill, J. Guo, K. L. VanDussen, R. C. Orchard, M. T. Baldridge, S. Lee, C. B. Wilen, Tuft-cell-intrinsic and -extrinsic mediators of norovirus tropism regulate viral immunity. *Cell Rep.* **41**, 111593 (2022).
28. H. Dubois, F. Sorgeloos, S. T. Sarvestani, L. Martens, Y. Saeys, J. M. Mackenzie, M. Lamkanfi, G. van Loo, I. Goodfellow, A. Wullaert, Nlrp3 inflammasome activation and gasdermin D-driven pyroptosis are immunopathogenic upon gastrointestinal norovirus infection. *PLOS Pathog.* **15**, e1007709 (2019).
29. A. J. Sharon, H. A. Filyk, N. M. Fonseca, R. L. Simister, R. B. Filler, W. Yuen, B. K. Hardman, H. G. Robinson, J. H. Seo, J. Rocha-Pereira, I. Welch, J. Neyts, C. B. Wilen, S. A. Crowe, L. C. Osborne, Restriction of viral replication, rather than T cell immunopathology, drives lethality in murine norovirus CR6-infected STAT1-deficient mice. *J. Virol.* **96**, e0206521 (2022).
30. B. A. Robinson, J. A. Van Winkle, B. T. McCune, A. M. Peters, T. J. Nice, Caspase-mediated cleavage of murine norovirus NS1/2 potentiates apoptosis and is required for persistent infection of intestinal epithelial cells. *PLOS Pathog.* **15**, e1007940 (2019).
31. J. G. Doench, N. Fusi, M. Sullender, M. Hegde, E. W. Vaimberg, K. F. Donovan, I. Smith, Z. Tothova, C. Wilen, R. Orchard, H. W. Virgin, J. Listgarten, D. E. Root, Optimized sgRNA design to maximize activity and minimize off-target effects of CRISPR-Cas9. *Nat. Biotechnol.* **34**, 184–191 (2016).
32. J. Lieberman, H. Wu, J. C. Kagan, Gasdermin D activity in inflammation and host defense. *Sci. Immunol.* **4**, eaav1447 (2019).
33. F. Shao, Gasdermins: Making pores for pyroptosis. *Nat. Rev. Immunol.* **21**, 620–621 (2021).
34. P. Broz, P. Pelegrin, F. Shao, The gasdermins, a protein family executing cell death and inflammation. *Nat. Rev. Immunol.* **20**, 143–157 (2020).
35. C. Rogers, T. Fernandes-Alnemri, L. Mayes, D. Alnemri, G. Cingolani, E. S. Alnemri, Cleavage of DFNA5 by caspase-3 during apoptosis mediates progression to secondary necrotic/pyroptotic cell death. *Nat. Commun.* **8**, 14128 (2017).
36. Z. Zhang, Y. Zhang, S. Xia, Q. Kong, S. Li, X. Liu, C. Junqueira, K. F. Meza-Sosa, T. M. Y. Mok, J. Ansara, S. Sengupta, Y. Yao, H. Wu, J. Lieberman, Gasdermin E suppresses tumour growth by activating anti-tumour immunity. *Nature* **579**, 415–420 (2020).
37. J. P. Borges, R. S. R. Saetra, A. Volchuk, M. Bugge, P. Devant, B. Sporsheim, B. R. Kilburn, C. L. Evavold, J. C. Kagan, N. M. Goldenberg, T. H. Flo, B. E. Steinberg, Glycine inhibits NINJ1 membrane clustering to suppress plasma membrane rupture in cell death. *eLife* **11**, e78609 (2022).
38. C. L. Evavold, J. Ruan, Y. Tan, S. Xia, H. Wu, J. C. Kagan, The pore-forming protein gasdermin D regulates interleukin-1 secretion from living macrophages. *Immunity* **48**, 35–44.e6 (2018).
39. B. N. Borin, W. Tang, T. J. Nice, B. T. McCune, H. W. Virgin, A. M. Krezel, Murine norovirus protein NS1/2 aspartate to glutamate mutation, sufficient for persistence, reorients side chain of surface exposed tryptophan within a novel structured domain. *Proteins* **82**, 1200–1209 (2014).
40. J. L. Hyde, S. V. Sosnovtsev, K. Y. Green, C. Wobus, H. W. Virgin, J. M. Mackenzie, Mouse norovirus replication is associated with virus-induced vesicle clusters originating from membranes derived from the secretory pathway. *J. Virol.* **83**, 9709–9719 (2009).
41. J. Song, R. D. Chow, M. A. Pena-Hernandez, L. Zhang, S. A. Loeb, E. Y. So, O. D. Liang, P. Ren, S. Chen, C. B. Wilen, S. Lee, LRRC15 inhibits SARS-CoV-2 cellular entry in trans. *PLoS Biol.* **20**, e3001805 (2022).
42. K. S. Bonham, M. H. Orzalli, K. Hayashi, A. I. Wolf, C. Glanemann, W. Weninger, A. Iwasaki, D. M. Knipe, J. C. Kagan, A promiscuous lipid-binding protein diversifies the subcellular sites of toll-like receptor signal transduction. *Cell* **156**, 705–716 (2014).
43. T. K. Phan, G. K. Bindra, S. A. Williams, I. K. H. Poon, M. D. Hulett, Combating human pathogens and cancer by targeting phosphoinositides and their metabolism. *Trends Pharmacol. Sci.* **40**, 866–882 (2019).
44. T. K. Phan, S. A. Williams, G. K. Bindra, F. T. Lay, I. K. H. Poon, M. D. Hulett, Phosphoinositides: Multipurpose cellular lipids with emerging roles in cell death. *Cell Death Differ.* **26**, 781–793 (2019).
45. S. L. Schaefer, G. Hummer, Sublytic gasdermin-D pores captured in atomistic molecular simulations. *eLife* **11**, e81432 (2022).
46. R. Kang, L. Zeng, S. Zhu, Y. Xie, J. Liu, Q. Wen, L. Cao, M. Xie, Q. Ran, G. Kroemer, H. Wang, T. R. Billiar, J. Jiang, D. Tang, Lipid peroxidation drives gasdermin D-mediated pyroptosis in lethal polymicrobial sepsis. *Cell Host Microbe* **24**, 97–108.e4 (2018).
47. M. Monteleone, A. C. Stanley, K. W. Chen, D. L. Brown, J. S. Bezbradica, J. B. von Pein, C. L. Holley, D. Boucher, M. R. Shakespear, R. Kapetanovic, V. Rolfes, M. J. Sweet, J. L. Stow, K. Schroder, Interleukin-1β maturation triggers its relocation to the plasma membrane for gasdermin-D-dependent and -independent secretion. *Cell Rep.* **24**, 1425–1433 (2018).
48. A. B. S. C. Garcia, K. P. Schnur, A. B. Malik, G. C. H. Mo, Gasdermin D pores are dynamically regulated by local phosphoinositide circuitry. *Nat. Commun.* **13**, 52 (2022).
49. A. L. Marat, V. Haucke, Phosphatidylinositol 3-phosphates-at the interface between cell signalling and membrane traffic. *EMBO J.* **35**, 561–579 (2016).
50. J. Hasegawa, B. S. Strunk, L. S. Weisman, PI5P and PI(3,5)P(2): Minor, but essential phosphoinositides. *Cell Struct. Funct.* **42**, 49–60 (2017).
51. J. L. Hyde, L. K. Gillespie, J. M. Mackenzie, Mouse norovirus 1 utilizes the cytoskeleton network to establish localization of the replication complex proximal to the microtubule organizing center. *J. Virol.* **86**, 4110–4122 (2012).
52. S. Vashist, L. Urena, M. B. Gonzalez-Hernandez, J. Choi, A. de Rougemont, J. Rocha-Pereira, J. Neyts, S. Hwang, C. E. Wobus, I. Goodfellow, Molecular chaperone Hsp90 is a therapeutic target for noroviruses. *J. Virol.* **89**, 6352–6363 (2015).
53. J. W. Goldman, R. N. Raju, G. A. Gordon, I. El-Hariry, F. Teofilivici, V. M. Vukovic, R. Bradley, M. D. Karol, Y. Chen, W. Guo, T. Inoue, L. S. Rosen, A first in human, safety, pharmacokinetics, and clinical activity phase I study of once weekly administration of the Hsp90 inhibitor ganetespib (STA-9090) in patients with solid malignancies. *BMC Cancer* **13**, 152 (2013).
54. S. Xia, Z. Zhang, V. G. Magupalli, J. L. Pablo, Y. Dong, S. M. Vora, L. Wang, T. M. Fu, M. P. Jacobson, A. Greka, J. Lieberman, J. Ruan, H. Wu, Gasdermin D pore structure reveals preferential release of mature interleukin-1. *Nature* **593**, 607–611 (2021).
55. W. J. Xie, S. Xia, A. Warshel, H. Wu, Electrostatic influence on IL-1 transport through the GSDMD pore. *Proc. Natl. Acad. Sci. U.S.A.* **119**, e2120287119 (2022).
56. A. Volchuk, A. Ye, L. Chi, B. E. Steinberg, N. M. Goldenberg, Indirect regulation of HMGB1 release by gasdermin D. *Nat. Commun.* **11**, 4561 (2020).
57. M. Edwards, "Norovirus NS1/2 Processing by Host Cell Caspases," thesis, University of Otago (2022).
58. S. Choi, J. K. Woo, Y. S. Jang, J. H. Kang, J. I. Hwang, J. K. Seong, Y. S. Yoon, S. H. Oh, Ninjurin1 plays a crucial role in pulmonary fibrosis by promoting interaction between macrophages and alveolar epithelial cells. *Sci. Rep.* **8**, 17542 (2018).
59. B. J. Ahn, H. Le, M. W. Shin, S. J. Bae, E. J. Lee, H. J. Wee, J. H. Cha, H. J. Lee, H. S. Lee, J. H. Kim, C. Y. Kim, J. H. Seo, E. H. Lo, S. Jeon, M. N. Lee, G. T. Oh, G. N. Yin, J. K. Ryu, J. K. Suh, K. W. Kim, Ninjurin1 deficiency attenuates susceptibility of experimental autoimmune encephalomyelitis in mice. *J. Biol. Chem.* **289**, 3328–3338 (2014).
60. F. Schwenk, U. Baron, K. Rajewsky, A cre-transgenic mouse strain for the ubiquitous deletion of loxP-flanked gene segments including deletion in germ cells. *Nucleic Acids Res.* **23**, 5080–5081 (1995).
61. H. M. Padilla-Nash, K. Hathcock, N. E. McNeil, D. Mack, D. Hoeppner, R. Ravin, T. Knutsen, R. Yonescu, D. Wangsa, K. Dorritie, L. Barenboim, Y. Hu, T. Ried, Spontaneous transformation of murine epithelial cells requires the early acquisition of specific

chromosomal aneuploidies and genomic imbalances. *Genes Chromosomes Cancer* **51**, 353–374 (2012).
62. H. Miyoshi, T. S. Stappenbeck, In vitro expansion and genetic modification of gastrointestinal stem cells in spheroid culture. *Nat. Protoc.* **8**, 2471–2482 (2013).
63. K. L. VanDussen, N. M. Sonnek, T. S. Stappenbeck, L-WRN conditioned medium for gastrointestinal epithelial stem cell culture shows replicable batch-to-batch activity levels across multiple research teams. *Stem Cell Res.* **37**, 101430 (2019).
64. R. C. Orchard, C. B. Wilen, J. G. Doench, M. T. Baldridge, B. T. McCune, Y. C. Lee, S. Lee, S. M. Pruett-Miller, C. A. Nelson, D. H. Fremont, H. W. Virgin, Discovery of a proteinaceous cellular receptor for a norovirus. *Science* **353**, 933–936 (2016).
65. S. Tyanova, T. Temu, P. Sinitcyn, A. Carlson, M. Y. Hein, T. Geiger, M. Mann, J. Cox, The Perseus computational platform for comprehensive analysis of (prote)omics data. *Nat. Methods* **13**, 731–740 (2016).
66. E. C. Meng, T. D. Goddard, E. F. Pettersen, G. S. Couch, Z. J. Pearson, J. H. Morris, T. E. Ferrin, U. C. S. F. ChimeraX, Tools for structure building and analysis. *Protein Sci.* **32**, e4792 (2023).
67. S. Bolte, F. P. Cordelieres, A guided tour into subcellular colocalization analysis in light microscopy. *J. Microsc.* **224**, 213–232 (2006).
68. J. F. Gilles, M. Dos Santos, T. Boudier, S. Bolte, N. Heck, DiAna, an ImageJ tool for object-based 3D co-localization and distance analysis. *Methods* **115**, 55–64 (2017).

**Acknowledgments:** We would like to thank P. Ren, S. Chen, M. Clark, and G. Lisi for helpful discussion. We acknowledge the Brown University CARE animal facility, the Flow Cytometry and Sorting Facility, the Genomics facility, the Leduc Bioimaging facility, and the Structural Biology Core Facility for help with critical analysis; the Washington University Genome Engineering & Stem Cell Center for CRISPR reagents and the Molecular Microbiology Imaging Facility for help with electron microscopy; the University of Texas Southwestern Proteomics Core for mass spectrometry analysis; I. Goodfellow for NS3, NS5, NS6, and NS7 antibodies; and S. H. Oh and S.-J. Bae for NINJ1 antibodies. Figures 2A and 3A and figs. S1A and S8Q were created with BioRender.com. **Funding:** This work was financially supported by the National Institutes of Health grant R01 AI183155 (S.L.), National Institutes of Health grant R21 AI173821 (S.L.), National Institutes of Health grant P20 GM109035 (S.L., J.R.W., and P.C.), National Institutes of Health grant K08 AI128043 (C.B.W.), National Institutes of Health grant R01 AI148467 (C.B.W.), National Institutes of Health grant K08 AI144033 (A.O.), National Institutes of Health grant R01 AI130020-01A1 (T.A.R.), National Institutes of Health grant U19 AI142784 (T.A.R.), National Institutes of Health grant P20 GM121344-05 (A.M.J.), National Institutes of Health grant R01 HL126887-04 (A.M.J.), National Institutes of Health grant R01 HL126887-05 (A.M.J.), National Institutes of Health grant R35 GM142684 (R.C.O.), National Institutes of Health grant R01 AI130055 (B.A.R. and T.J.N.), Smith Family Awards Program for Excellence in Biomedical Research (S.L.), Charles H. Hood Foundation Child Health Research Awards (S.L.), Burroughs Wellcome Fund Career Award for Medical Scientists (C.B.W.), Cancer Prevention and Research Institute of Texas grant RP200118 (T.A.R.), Pew Scholars Program (T.A.R.), and Welch Foundation (T.A.R.). **Author contributions:** Conceptualization: J.S., A.F., A.M.J., R.C.O., A.O., T.A.R., and S.L. Methodology: J.S., L.Z., S.M., A.F., B.A.R., T.A.R., and S.L. Investigation: J.S., L.Z., S.M., A.F., N.G., J.R.W., M.M.A., M.S.S., W.L.B., and S.L. Validation: J.S., A.F., N.G., P.C., W.L.B., and S.L. Visualization: L.Z., W.L.B., and S.L. Formal analysis: J.S., L.Z., N.G., and S.L. Resources: G.W., N.G., S.A.L., R.C.O., B.A.R., T.J.N., C.B.W., T.A.R., and S.L. Funding acquisition: S.L., C.B.W., and T.A.R. Project administration: S.L. Data curation: S.L. Software: S.L. Supervision: S.L. and T.A.R. Writing—original draft: J.S., S.M., and S.L. Writing—review and editing: J.S., L.Z., A.F., G.W., J.R.W., M.S.S., W.L.B., A.M.J., R.C.O., C.B.W., A.O., T.A.R., and S.L. **Competing interests:** The authors declare that they have no competing interests. **Data and materials availability:** All data needed to evaluate the conclusions in the paper are present in the paper and/or the Supplementary Materials. CRISPR screening data generated in this study are provided as table S1, and the raw FASTQ files can be found at the NCBI Sequence Read Archive (SRA) under BioProject PRJNA1043130.

Submitted 21 November 2024
Accepted 28 January 2025
Published 28 February 2025
10.1126/sciadv.adu7985